

Synthesis, Structure and Optical Memory Properties of Copper(I) Thiocyanate
Networks with Aromatic Amines, Diimines and Alkyl Sulfides

Gerardo Ayala

Annandale, Virginia

Bachelor of Science in Chemistry, College of William and Mary, 2014

A Thesis presented to the Graduate Faculty
of the College of William and Mary in Candidacy for the Degree of
Master of Science

Department of Chemistry

The College of William and Mary
May 2016

APPROVAL PAGE

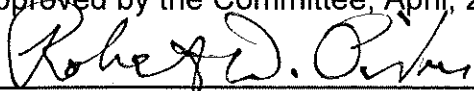
This Thesis is submitted in partial fulfillment of
the requirements for the degree of

Master of Science




Gerardo Ayala

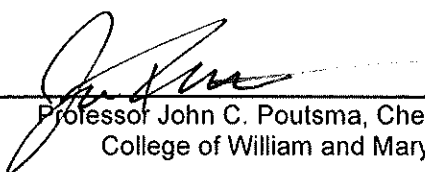
Approved by the Committee, April, 2016



Committee Chair
Professor Robert D. Pike, Chemistry
College of William and Mary



Professor Beborah C. Bebout, Chemistry
College of William and Mary



Professor John C. Poutsma, Chemistry
College of William and Mary

ABSTRACT

A series of CuSCN compounds were synthesized. Ligands included the alkyl sulfides methyl sulfide (Me_2S), ethyl sulfide (Et_2S), isopropyl sulfide (Pr_2^iS) and tetrahydrothiophene (THT); diimine ligands pyrazine (Pyz), 2,3-dimethylpyrazine (2,3-Me₂Pyz), 2,5-dimethylpyrazine (2,5-Me₂Pyz), 2-aminopyrazine (2-NH₂Pyz) and 2-methoxypyrazine (2-MeOPyz); two-ring diimines quinoxaline (Qox), quinazoline (Qnz), phthalazine (Ptz); and 3-halopyridines 3-chloropyridine (3-ClPy), 3-bromopyridine (3-BrPy), 3-iodopyridine (3-IPy). Crystal structures were solved for twelve products. With the exception of one Cu(II) compound, all could be classified in the common motifs of chains, ladders or sheets. Alkyl sulfides formed either 1:2 (CuSCN)₂L 1-D chains (L = Me_2S , **1a** and THT, **4**) or 1:1 (CuSCN)₂L 1-D ladders (L = Et_2S , **2** and Pr_2^iS , **3**) when reacted with CuSCN. New compounds of CuSCN with diimine ligands included two 2:1 (CuSCN)₂LL 2-D bridged ladders (LL = Qox, **5** and 2-NH₂Pyz, **8**), two (CuSCN)₂L 1:1 2-D sheets (L = Qnz, **6** and 2-MeOPyz, **9**) and one 1:1 (CuSCN)₂LL 2-D sheet (Ptz, **7**). Structures of the known 1:2 (CuSCN)₂L compounds, where L = 3-ClPy (**15a**) or 3-BrPy (**16**) were solved as 1-D chains.

Optical memory experiments sought to rapidly and significantly reduce the peak intensity in the ultraviolet/visible (UV/Vis) emission spectra of the synthesized compounds as a means of storing binary information. Fully emissive states were assigned as “unwritten,” while states with reduced emission were assigned as “written.” Samples were exposed to a high-energy tunable UV laser at 80 K for five minute intervals in order to affect emission intensities. Recovery capabilities were assessed by warming the samples to 298 K, allowing them to reach thermal equilibrium, and cooling them to 80 K before obtaining final scan. The known compounds (CuSCN)₂LL, where LL = 2,3-dimethylpyrazine (2,3-Me₂Pyz, **11**), 2,5-dimethylpyrazine (2,5-Me₂Pyz, **12**) demonstrated reduced emission after irradiation, but suffered from fatigue after only one write/read/erase cycle. Compound **16** proved the most promising, displaying both significant emission depletion and complete recovery of initial intensity after three cycles. The x-ray crystal structure of **16** indicates numerous close carbon-bromine and sulfur-bromine interactions. Combined with computational calculations indicating an elongation of the pyridine C-Br bond in the most probable excited state, it is plausible that structural features play a role in the optical memory behavior of this compound.

TABLE OF CONTENTS

Acknowledgements	ii
Dedications	iii
List of Tables	iv
List of Figures	v
Introduction	1
Experimental	15
Materials	15
Instrumentation	15
Syntheses	17
Optical Memory Experiments	23
Results and Discussion	24
Synthesis and Characterization	24
Structures of CuSCN-Alkyl Sulfide Compounds	29
Structures of CuSCN-Diimine Compounds	35
Structures of CuSCN-3-XPy Compounds	44
Optical Memory Results	52
Conclusion	61
Appendix	62
References	71

ACKNOWLEDGEMENTS

First, I would like to thank Professor Robert D. Pike for giving me the opportunity both as an undergraduate and a graduate student to work in his lab and hone my skills in chemistry and research. I have come out with a much more firm grasp on many lab techniques and a much greater appreciation of the discipline. Thank you also to Professors Deborah C. Bebout and John C. Poutsma for reviewing this manuscript and for agreeing to form part of my defense committee. Additionally, I would like to thank Dr. Howard H. Patterson and Aaron Nicholas at the University of Maine for their work on the optical memory experiments and computations.

I would also like to express my immense appreciation for my fellow research students and colleagues: the members of the Pike Lab, past and present, who have helped me both as an undergraduate and a graduate student. Special thanks go to Kylie Henline for helping me get on my feet as a new research student, and Kathy Huynh, who has been an immense help both in my academic life and life in general outside the lab.

I must also express my gratitude to the donors who have made my eleven (!) semesters and two summers at the College possible. Quite simply, I would not have been able to attend this amazing institution without their generosity. Thank you to everyone who has contributed to the William and Mary Scholars Award, the James Monroe Scholars program, and the various other scholarships and awards I have been selected for.

This Thesis is dedicated to my family: my father, Gerardo Ayala Sr., my mother, Aracely Haydee Fonseca de Ayala, my older sister Ana Maria Ayala, and my younger sister Stephanie Ayala. They have supported me throughout my academic career, and I hope to repay their love and assistance in the coming years.

LIST OF TABLES

1. Summary of Compounds Studied	24
2. Close Interactions in (CuSCN)Qnz	37
3. Close Interactions in Structure of (CuSCN)(3-ClPy) ₂	47
4. Close Interactions in Structure of (CuSCN)(3-BrPy) ₂	51
5. Peak Emission Intensities of (CuSCN) ₂ (2,3-Me ₂ Pyz)	53
6. Peak Emission Intensities of (CuSCN) ₂ (2,5-Me ₂ Pyz) after One, Two, and Three Write/Read/Erase Cycles	54
7. Peak Emission Intensities of (CuSCN)(3-BrPy) ₂ after One, Two, and Three Write/Read/Erase Cycles	57

LIST OF FIGURES

1. Potential Networking of a Metal Salt	2
2. Phases of Copper(I) Thiocyanate	3
3. Networking of (CuSCN)(Quinoline) ₂ and (CuSCN)(2,6-Me ₂ Py)	4
4. Common Network Types of CuSCN	5
5. Fusions of CuSCN Rings	6
6. Networking Examples of CuSCN with Bridging Diimines	7
7. Networking Examples of Two CuX-Sulfide Compounds	9
8. Schematic of an Optical Memory Process	10
9. Potential Organic Optical Memory Compounds	11
10. Unwritten “off” form of a Ru(II)-diimine Complex	12
11. Ligands used in CuSCN-L Syntheses	14
12. Powder X-ray diffraction Pattern of Two CuSCN-Me ₂ S Compounds	25
13. Thermogravimetric Traces of CuSCN-Sulfide Compounds	26
14. Thermogravimetric Traces of CuSCN-Diimine Compounds	28
15. Structural Diagrams of (CuSCN)(Me ₂ S) ₂	30
16. Structural Diagrams of (CuSCN)(Et ₂ S)	31
17. Diagram of Disorder in (CuSCN)(Et ₂ S)	32
18. Structural Diagram of (CuSCN)(Pr ⁱ ₂ S)	33
19. Structural Diagrams of (CuSCN)(THT) ₂	34
20. Structural Diagrams of (CuSCN) ₂ Qox	36
21. Structural Diagrams of (CuSCN)Qnz	38
22. Thermal Ellipsoid Rendering of (CuSCN) ₂ Ptz	39
23. Networking Diagrams of (CuSCN) ₂ Ptz	40

24. Asymmetric Unit of $(\text{CuSCN})_2(2\text{-NH}_2\text{Pyz})$	41
25. Networking Diagrams of $(\text{CuSCN})_2(2\text{-NH}_2\text{Pyz})$	42
26. Asymmetric Unit and Disorder of $(\text{CuSCN})(2\text{-MeOPyz})$	43
27. Networking of $(\text{CuSCN})(2\text{-MeOPyz})$	44
28. Structural Diagrams of $(\text{CuSCN})(3\text{-ClPy})_2$	45
29. Canting of 3-ClPy ligands in $(\text{CuSCN})(3\text{-ClPy})_2$	46
30. Comparison of $(\text{CuSCN})(3\text{-ClPy})_2$ and $(\text{CuSCN})(3\text{-BrPy})_2$	48
31. Structural Diagrams of $(\text{CuSCN})(3\text{-BrPy})_2$	49
32. Canting of 3-BrPy ligands in $(\text{CuSCN})(3\text{-BrPy})_2$	50
33. Diagrams of $\text{Cu}(\text{SCN})_2(3\text{-ClPy})_4$	52
34. Emission Spectrum of $(\text{CuSCN})_2(2,3\text{-Me}_2\text{Pyz})$	53
35. Emission Spectra of $(\text{CuSCN})_2(2,5\text{-Me}_2\text{Pyz})$	55
36. Emission Spectra of $(\text{CuSCN})(3\text{-BrPy})_2$	58
37. Emission Spectrum of $(\text{CuSCN})(3\text{-IPy})$	60

Introduction

Polymeric metal-organic networks have been the subjects of research not only for the immense number of unique structures they exhibit, but also for the variety of potential applications. Porous metal-organic frameworks have garnered interest as gas storage or chemical separation materials.^{1,2} Research of catalytic applications seeks to exploit the transition metal centers' flexible redox states and binding capabilities,³ while other metal-organic compounds could be designed to act as chemo- or photosensors and memory materials.^{4,5} The photophysical properties of metal-organic networks can vary greatly even within a series of very similar metal-ligand combinations. This is especially true for the d^{10} metals copper(I) and silver(I), which have long been the subject of luminescence studies.^{4,5} Metal-organic networks often form by self-assembly under modest thermal conditions, and can be isolated quite easily by precipitation from the reaction mixture. As multiple products may form in these self-assembly reactions, stoichiometric control of metal:ligand ratios and/or reaction conditions must be employed to obtain desired compounds.

Metal salts containing inner-sphere anions such as halides, pseudohalides and chalcogenides form inorganic networks. Addition of organic ligands transforms the metal salt networks, with the resulting network type depending on the ligand added. Monodentate ligands tend to result in networks of one or two dimensions, and occasionally monomers. Addition of bridging ligands, on the other hand, can result in numerous two- and three-dimensional topologies.

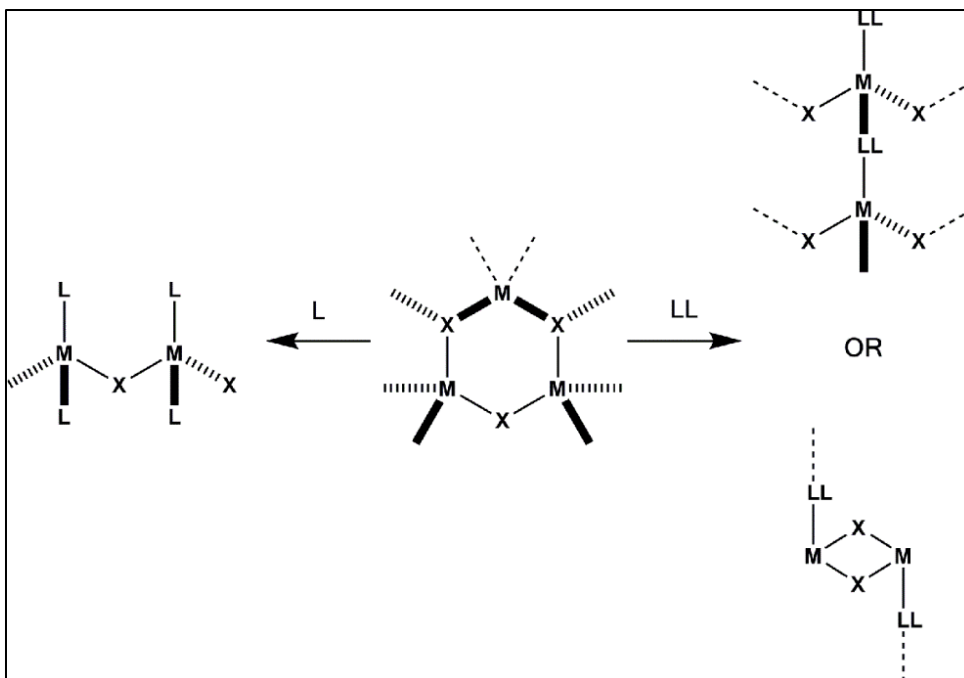


Figure 1. Networking of a hypothetical metal salt CuX.

Copper(I) thiocyanate (CuSCN) is one example of an inner-sphere metal salt. It forms inorganic networks itself in three known polymorphs.⁶⁻⁸ All three polymorphs are composed of cross-linked CuSCN and CuS chains, forming elongated hexagonal CuSCN rings and hexagonal Cu_3S_3 rings. The three phases of CuSCN are shown in Figure 2. The three-dimensional polymorphs arise from the bridging capabilities of the sulfur atom of the thiocyanate, which acts as a four-coordinate μ_3 -bridge between the four-coordinate Cu centers. The hexagonal CuSCN rings are comparable to the hexagonal wurtzite form of CuI , although the thiocyanate anion elongates the rings. Each phase also contains a Cu_3S_3 hexagonal ring motif; the α -phase ring is more irregular compared to the symmetrical β -phase rings.

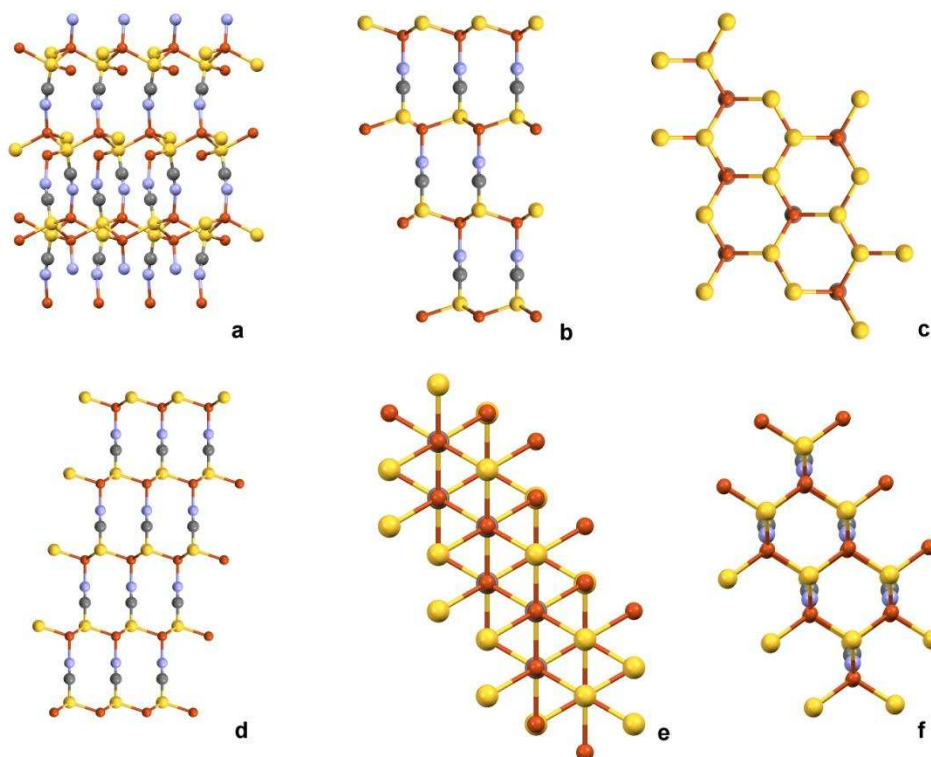


Figure 2: CuSCN phases; (a) α -phase, viewed down the b -axis; (b) β -phase, viewed down the b -axis; (c) β -phase, viewed down the c -axis; (d) β high-temperature phase, viewed down the b -axis; (e) β high-temperature phase, viewed down the c -axis; (f) β high-temperature phase, oriented to show hexagonal Cu_3S_3 rings.

Copper(I) thiocyanate has been shown to react readily with soft ligands such as organic amines and sulfides. As previously mentioned, the nature of the ligand greatly influences the resulting network. Reactions of CuSCN with monodentate capping ligands, such as pyridine (Py) and tetrahydrothiophene (THT), often form one or two-dimensional networks; three common types include chains (A and A'), ladders (B), and sheets (C) see Figure 4. Type A networks consist of CuSCN chains linked by μ_2 -(N,S)-thiocyanate, with the copper coordination sphere completed by pairs of ligand molecules or by a single molecule (A or A' respectively). Many Py-containing CuSCN networks of type A have been reported, with $\text{L} = 2\text{-MePy}$ (Me = methyl), 3-MePy, 4-MePy, 4-EtPy (Et

= ethyl), 2,4-Me₂Py, and quinoline.^{9,10} Type A' networks have been reported with larger ligands such as L = 2,6-Me₂Py and 2,4,6-Me₃Py.^{9,10}

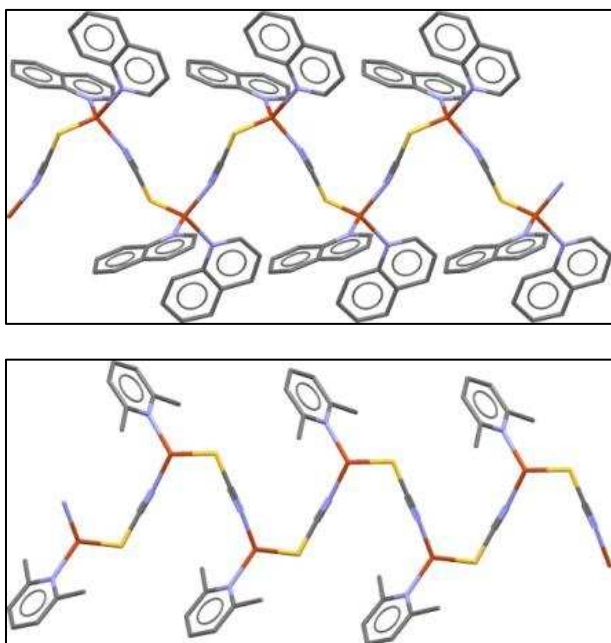


Figure 3. Networking of (CuSCN)(Quinoline)₂, a Type A network (top) and (CuSCN)(2,6-Me₂Py), a type A' network (bottom). Both shown as wire frame diagrams. Color scheme X-ray structures: orange = Cu, grey = C, blue = N, red = O, yellow = S, brown = Br, green = Cl.

Type B networks consist of two antiparallel CuSCN chains connected by μ_3 -(S,S,N) thiocyanate bridging. This results in the formation of fused, alternating Cu₂S₂ dimers and Cu₂(SCN)₂ rings. Networks of this type have been found for L = 2-MePy, 2-EtPy, and N-methylpiperidine.⁹ Type C networks are likewise formed by crosslinking of chains in two directions by μ_3 -(S,S,N) thiocyanate, resulting in rippled sheets of hexagonal Cu₃(SCN)₂S rings. Two sheet motifs have been observed: *cis*-fused sheets (L = N-methylmorpholine) and *trans*-fused (L = 3-ClPy, 3-BrPy).¹⁰ These sheet patterns are shown in Figure 5. When viewed edgewise, *cis*-fused sheets appear as square waves; *trans*-fused sheets, on the other hand, exhibit a zigzag pattern.

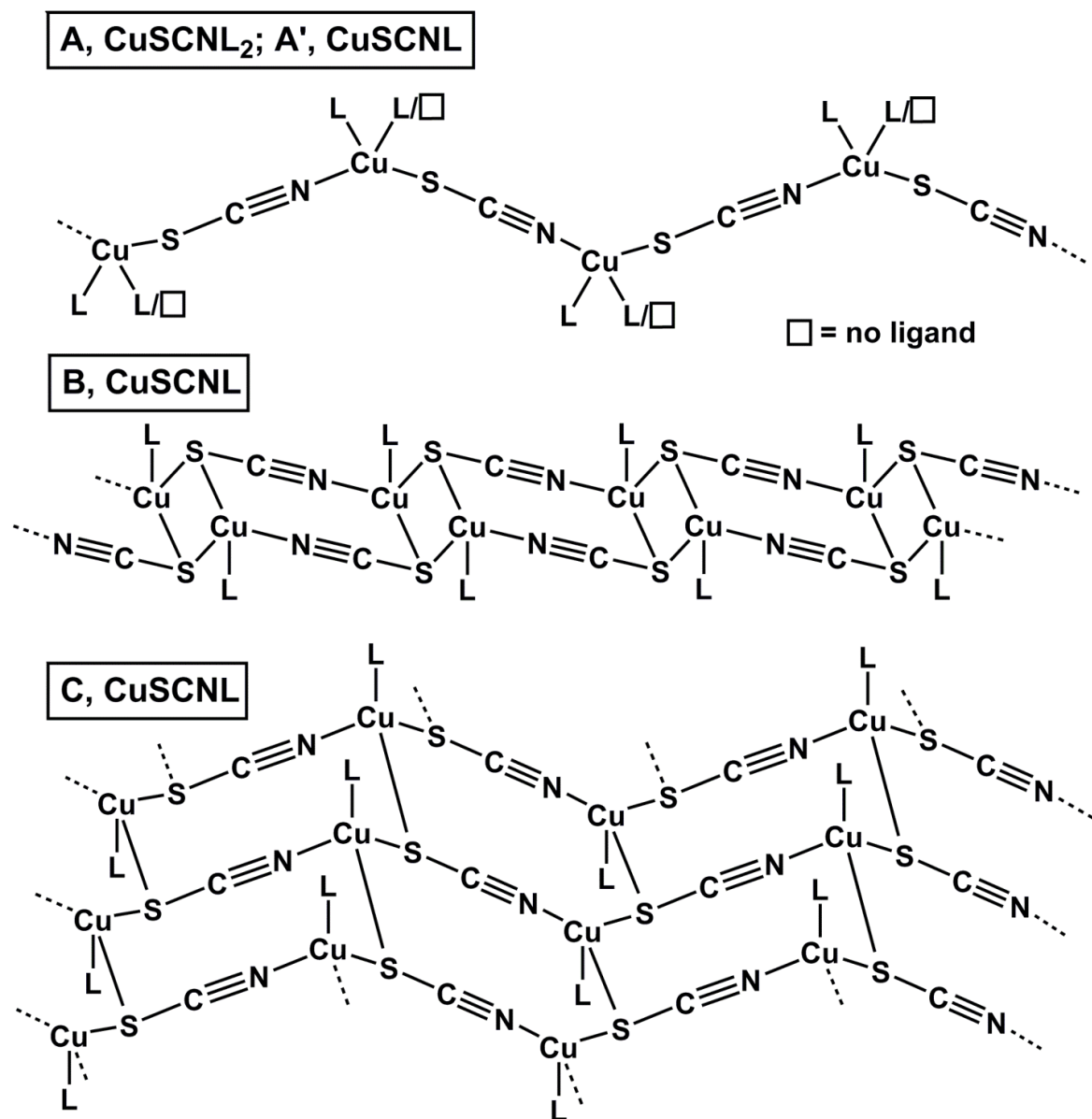


Figure 4. Common network types of CuSCN-L .

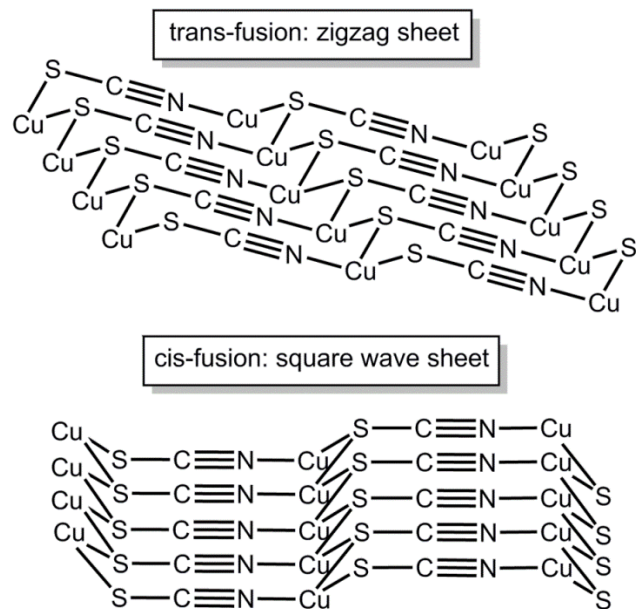


Figure 5. Ring fusions of hexagonal CuSCN sheets.

Bridging ligands can be used to form expanded versions of network types A, B and C. Bidentate pyrazines (Pyz) have been shown to form 2D Type A networks, where the organic ligand bridges chains through copper centers. Networks of this type are seen in $(\text{CuSCN})\text{LL}$ complexes where LL = Pyz or 2-MePyz.^{11,12} For $(\text{CuSCN})_2\text{LL}$ complexes, both bridged 2D Type B ladders and 3D Type C networks have also been reported. Ladders have been observed for LL = 2-MePyz¹³ and several large amine ligands.¹⁸ *Trans*-fused sheets containing Pyz or 2,5-Me₂Pyz¹⁴⁻¹⁶ and *cis*-fused sheets containing 2-Me-3-EtPyz¹⁷ have likewise been reported. Two examples of CuSCN with bridging ligand are shown in Figure 6 below.

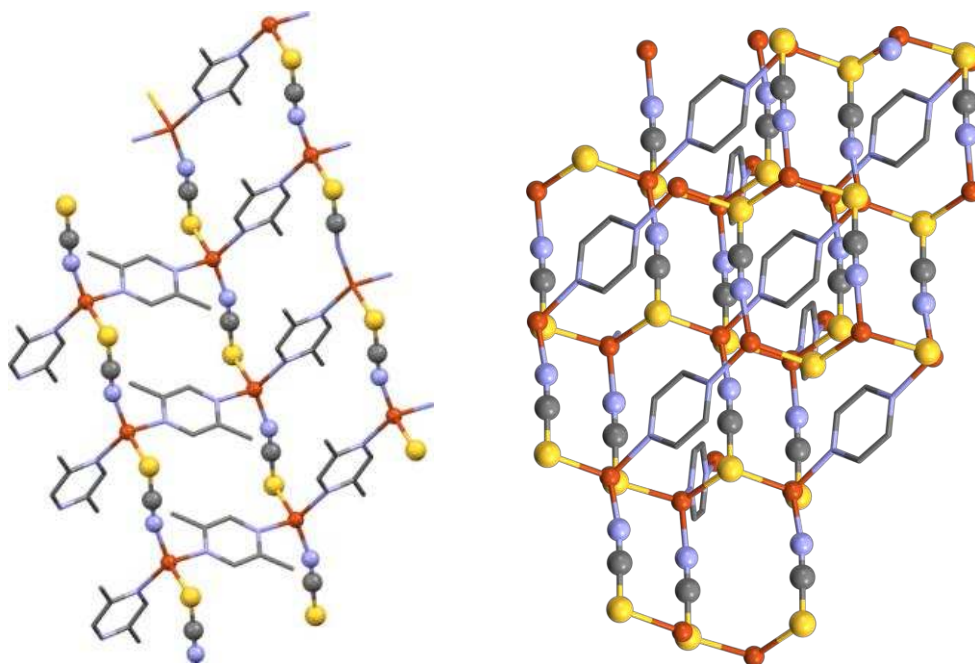


Figure 6. Left, $(\text{CuSCN})(2,5\text{-Me}_2\text{Pyz})$, a 2D type A network. Right, $(\text{CuSCN})_2\text{Pyz}$, a 3D Type C network. Hydrogen atoms omitted.

$(\text{CuSCN})_2\text{LL}$ complexes may also exhibit different network types. One such network is composed of Cu_2S_2 dimers linked by SCN and LL. As seen in the compounds $(\text{CuSCN})_2(2,3\text{-Me}_2\text{Pyz})$ and $(\text{CuSCN})_2(3\text{-IPyz})$, each dimer is connected to six other dimers.^{19,20} The $\mu_3\text{-S}$ atoms of each dimer are connected to another dimer as part of a CuSCN chain, while each Cu center is connected to two other dimers by NCS and by a bridging Pyz ligand. This type of networking bears some resemblance to type B ladders, where one of the $\text{Cu}_2(\text{SCN})_2$ “rungs” is opened up and binds in a different direction. This results in a larger 16-membered $(\text{CuSCN})_4$ macrocycle. Some Pyz ligands, including 2-NCPyz, fail to bridge Cu centers, instead forming the Type A compound $(\text{CuSCN})(2\text{-NCPyz})_2$.¹³

Reactions of CuSCN and other potentially bridging amine ligands can also result in different networking. Pyrimidines (Pym), containing a 120° “bite” angle, sometimes act as monodentate capping ligands, resulting in the formation of Type A or Type C

networks. Examples include the Type A compound $(\text{CuSCN})(4\text{-HOPym})_2$,¹³ as well as the Type C, *trans*-fused $(\text{CuSCN})(4\text{-MePym})$ ¹² and $(\text{CuSCN})(5\text{-BrPym})$.¹³ The compound $(\text{CuSCN})_2\text{Pym}$ exhibits an entirely different type of connectivity; CuSCN chains intersect to form large 18-membered macrocycles, with the bidentate Pym ligand bridging between cycles and forming smaller 10-membered $\text{Cu}_3\text{S}_2\text{C}_2\text{N}_3$ rings. Another unique network is created by $(\text{CuSCN})_2(4\text{-MePym})$.¹³ This network contains numerous fused motifs: both *cis* and *trans*-fused CuSCN sheets, Cu_3S_3 rings, a small 10-membered ring including the ligand, and a very large CuSCN and ligand channel. Compounds of CuSCN and pyridazines (Pdz) have not been extensively studied; only the network of the parent ligand, Pdz, is known, a 2D *cis*-fused sheet containing the monodentate ligand.²¹

Organosulfur compounds constitute another noteworthy class of soft ligands. The additional bonding capability as π -donors and π -acceptors, as well as the additional lone pair on sulfur open up the possibility of increased bridging between metal centers. Sulfides can also act as solubilizing agents for sparingly soluble Cu(I) salts in organic reactions.²² Metal-organic networks containing several types of organosulfur ligands have been extensively studied, including sulfides, thiolates, thioamides, and phosphine sulfides.²³⁻²⁶ Structural motifs of CuX ($\text{X} = \text{Cl}, \text{Br}, \text{I}, \text{CN}$) and these ligands include Cu_2X_2 dimers, Cu_2X_2 ladders, and numerous polymers and oligomers. Some combinations of metal salts and organosulfides produce several structures, as is the case for CuI and THT.^{22a}

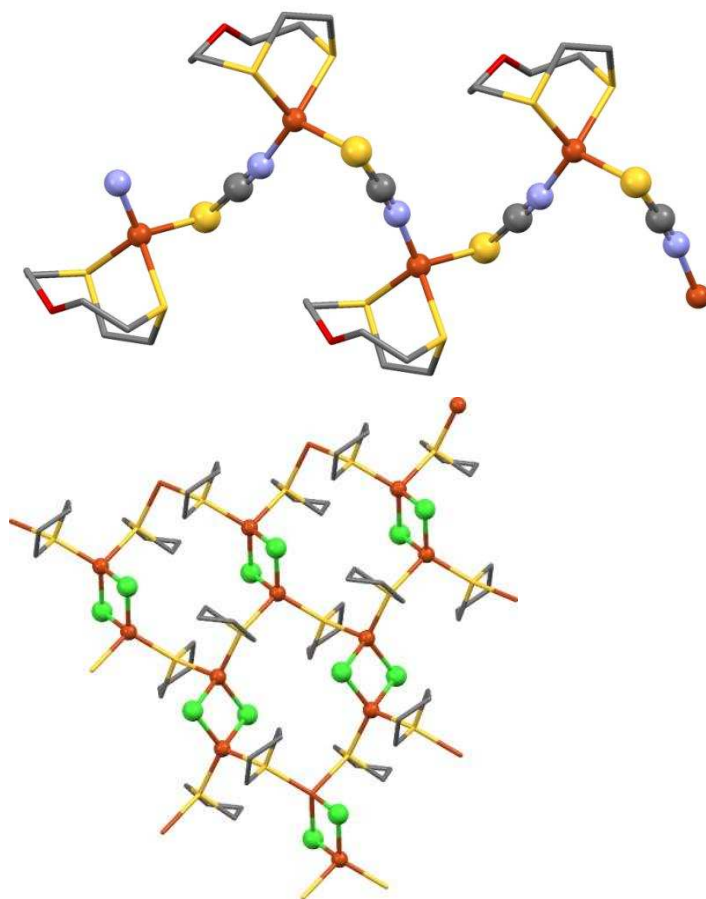


Figure 7. Top, $(\text{CuSCN})(1,4\text{-dithia-7-oxacyclononan-1,4-diyl})$, a 1-D chain of CuSCN and bidentate cyclic thioether.²³ⁱ Bottom, networking of sulfide-bridged Cu_2Cl_2 dimers in $(\text{CuCl})_2\text{THT}_2$.²⁷

Surprisingly little research has been published on CuSCN with simple aliphatic sulfides. The most notable networks found contained one of two cyclic thioethers: $(\text{CuSCN})(1,10\text{-dithia-18-crown-6-ether})$, a Type B ladder network,²³ⁱ and $(\text{CuSCN})(1,4\text{-dithia-7-oxacyclononan-1,4-diyl})$, a Type A network with a single bidentate sulfur ligand per copper.^{23d} In both compounds, the hard oxygen atom(s) fail to coordinate with the soft Cu centers. Reported thioamide and phosphine sulfide compounds of CuSCN form various ring and bridged chain motifs rather than networks Types A, B or C.^{24b,24c,26a,}

The intense luminescence of emissive solid compounds, including many metal-organic networks, can potentially be harnessed in information storage devices. The

premise of so-called “optical memory,” or the reading and writing of information using electromagnetic radiation, is to induce a binary and reversible photophysical change in a material. The change in the observed photophysical property, often fluorescence from a specific excitation wavelength, can be detected as a drop in emission intensity, a change in the emission peak wavelength, or emission from an otherwise non-emissive compound. Figure 8 shows a schematic of a write/read/erase process.

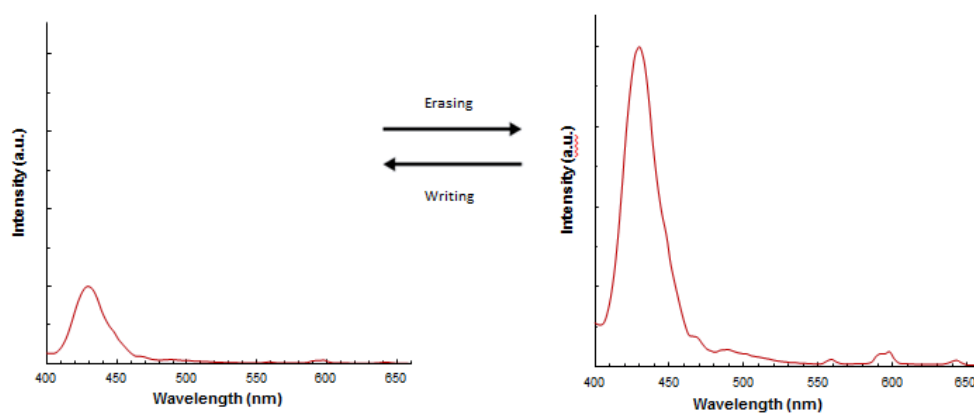


Figure 8. Optical memory process scheme.

A wide array of organic and inorganic compounds can potentially behave as the optical memory materials. Some classes of organic compounds that have been the subject of optical memory studies include spiropyrans,^{28,29} polycyclic aromatic compounds such as anthracenes,³⁰ fulgides, and fulgimides,³¹⁻³³ and combined systems.³³

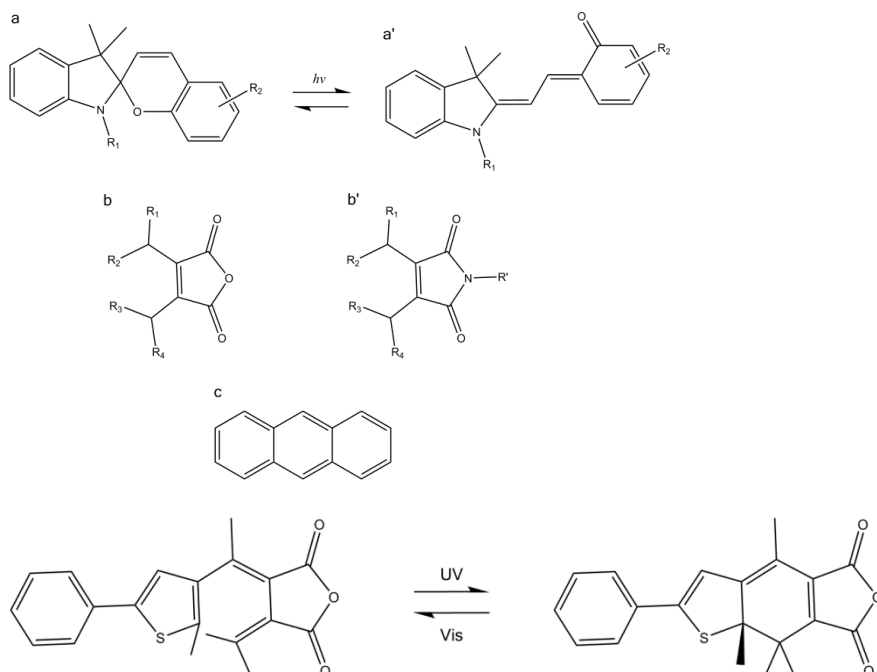


Figure 9. Top, classes of organic compounds used in optical memory studies: a and a', ring-closed and ring-open spiropyrans; b, diagram of a fulgide; b' diagram of a fulgimide; c, anthracene. Bottom, open ('0') and closed ('1') forms of Phenyl-Thiophen-Fulgide from Reference 31.

These compounds undergo a photochemical reaction from the “blank” or “off” form (zero in binary) to the “written” or “on” form (representing a one). Stability of both forms is key; spiropyrans were found to have stable blank forms but thermally unstable written forms,³⁰ precluding their use as permanent storage. Fulgides and fulgimides were meanwhile found to be stable in both forms, and resistant to photobleaching after large numbers of write/erase cycles.^{31,33}

Optical memory in fully inorganic systems has also been reported. Cu^+ and Ag^+ -doped β -alumina crystals were found to exhibit notably different emission wavelengths after irradiation of a certain portion of a crystal with 351 nm laser light during cooling.⁵ Irradiated spots emitted orange, a result of the formation of $[\text{CuAg}]^+$ dimers, while unexposed areas emitted green. Omary and Patterson also reported the memory

phenomena observed in the emission spectra of $\text{K}_2\text{Na}[\text{Ag}(\text{CN})_2]_3$.³⁴ In this instance, the lower energy (LE) peak in the emission spectrum of the compound is replaced by an intermediate energy (IE) peak, and the intensity of the high energy peak (HE) is greatly diminished. Warming of the compound and cooling it to the experimental temperature (70 K) led to recovery of the intensity of the HE peak, and the reemergence of the LE peak; the IE peak completely vanished.³³ Finally, metal-organic compounds have proven yet another avenue for optical memory. Tyson, Bignozzi and Castellano reported the optical memory behavior of a Ru(II)-diimine complex, where one of the diimines is substituted with a photo-reactive dianthryl unit (see Figure 8).³⁵

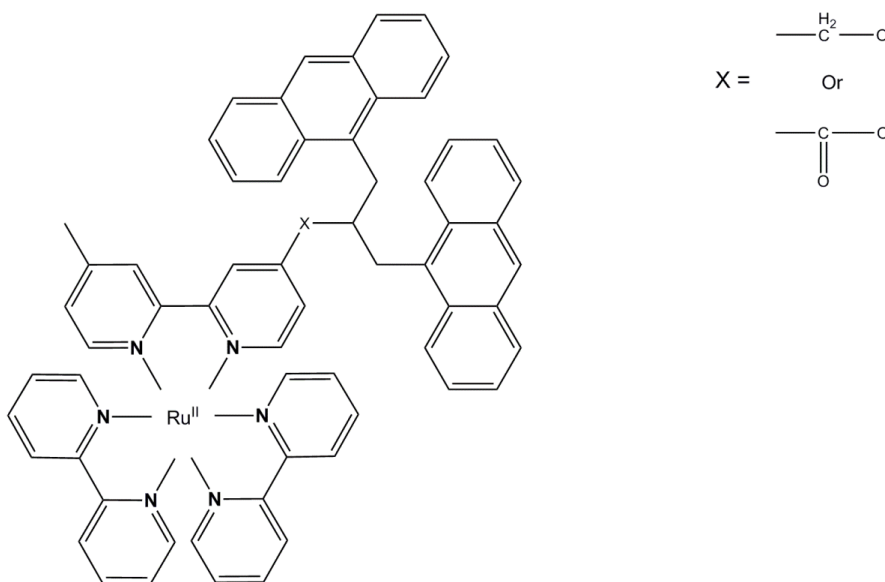


Figure 10. Off form of Ru(II)-diimine complex from Reference 35.

The uncyclized dianthryl unit is responsible for the quenching of metal-to-ligand charge transfer (MLCT) emission from excited states.³⁵ When cyclized using 390 nm light, the dianthryl is no longer a pathway for relaxation from excited states, and MLCT emission pathway is “activated.”

Numerous challenges preclude the application of many of the above compounds in digital storage devices. Thermal stability of both off and on states (zero or one), as

mentioned with regard to spiropyrans, constitutes one major hurdle. The conditions of the write/read/erase process should not be too extreme; the requirement of cooling and simultaneously writing into the Cu^+/Ag^+ -doped β "-alumina crystals likely eliminates them as useful information storage material,⁵ as well as the homogenous $\text{K}_2\text{Na}[\text{Ag}(\text{CN})_2]_3$ crystals. Dvornikov outlines a number of desirable properties that should be achieved by potential optical memory compounds: large information storage density (bits/unit volume); random and parallel access (should be able to retrieve information from anywhere in the device or in successive bits); fast writing and reading rates (10^{-6} s); small size and low cost; minimal cross talk between adjacent bits (bits should not interact); high reading sensitivity.³² Additionally, Castellano and Dvornikov both note that to prevent destructive and/or confounded read out of information from a written molecule, the following considerations should be taken in designing a molecular system: (1) the "off" form should absorb neither the wavelength of the reading laser nor the emitted wavelength of written molecules; (2) the reading wavelength should not cause the "on" form to be turned off; and (3) the erasing wavelength must be different from both the writing and reading wavelengths.^{33,35} These specific recommendations apply to systems using multiple wavelengths for the write/read/erase process, but similar considerations must be taken for systems utilizing other erasure procedures.

The work presented herein pertains to the structural and luminescent properties of CuSCN networks with aromatic amine, diimine or alkyl sulfide ligands. A total of thirteen new CuSCN compounds were synthesized, containing the following ligands: alkyl sulfides methyl sulfide (Me_2S), ethyl sulfide (Et_2S), isopropyl sulfide (Pr_2S) and THT; two-ring diimines quinoxaline (Qox), quinazoline (Qnz), phthalazine (Ptz); and monosubstituted pyrazines 2-aminopyrazine (2- NH_2Pyz) and 2-methoxypyrazine (2-MeOPyz).

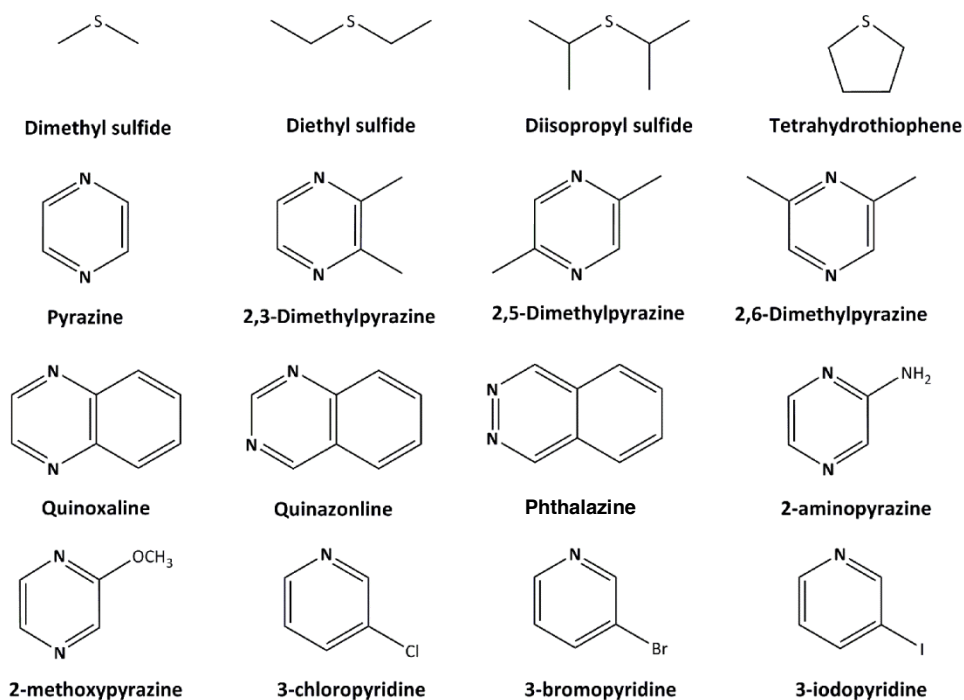


Figure 11. Aromatic amine and alkyl sulfide ligands used.

Additionally, six known CuSCN-aromatic amine compounds were produced for optical memory experiments, with ligands 3-ClPy, 3-BrPy, Pyz, 2,3-Me₂Pyz, and 2,5-MePyz. New crystal structures were obtained for twelve compounds. Six CuSCN-amine networks were subjected to UV/VIS spectroscopy and optical memory experiments to determine their potential as information storage materials. The non-luminescent CuSCN-alkyl sulfide networks were not used in these experiments; only their synthesis and structures are reported here. Most of the new structures were found to fall under one of the network types outlined in Chart 1. Four Type A chains, four Type B ladders, three Type C sheets, and one monomer were solved.

Experimental

Materials

All reagents were purchased from Sigma-Aldrich or Acros. Commercial CuSCN was shown by FTIR to consist solely of the α -phase.³⁸ Quinoxaline was purified by sublimation prior to use. All other reagents were used as purchased without additional purification.

Instrumentation

Infrared Spectroscopy

IR spectra were collected on a Shimadzu IRTracer-100 instrument using a diamond ATR probe. The following parameters were used: scanning range, 4000-450 cm^{-1} ; number of scans, 12; resolution, 4; apodization, Happ-Genzel; intensity mode, absorbance.

Chemical Analysis

Analyses for C, H, and N were carried out by Atlantic Microlabs, Norcross, GA. Atomic absorption analyses for copper content were carried out using a Perkin-Elmer AAnalyst 700 equipped with a copper hollow cathode lamp. The method was as follows: 11.0-13.0 mg of sample was measured in a 2-dram vial and digested with 25 drops of concentrated nitric acid. The vial was sealed and heated for five minutes in a warm bath. To the warm green solution, about 2 mL of deionized (DI) water was added. The resulting solution was quantitatively transferred to a clean 100 mL volumetric flask using a Pasteur pipette. The vial containing the acidic sample solution was rinsed twice with 2 mL DI water, with each rinsing being transferred to the 100 mL volumetric flask with the same Pasteur pipette. The volumetric flask was diluted to the 100 mL mark and mixed thoroughly by inversion. Depending on predicted copper content, 1 or 2 mL of the solution in this flask was transferred to a second, 25 mL volumetric flask. After diluting to volume, the flask was mixed by inversion. 500, 1000, 1500, 2000, and 2500 ppb

standards were prepared and used to generate a calibration curve before analyzing samples.

Thermogravimetric Analysis

Thermogravimetric analyses (TGA) were conducted on a platinum pan using a TA Instruments Q500 in the dynamic (variable temp.) mode with a maximum heating rate of 50 °C/min. to 800 °C under 50 mL/min. N₂ flow. Aliphatic sulfides compounds were taken only to 500 °C because ligand loss took place well below this temperature.

Single-crystal X-ray Diffraction

All measurements were made using graphite-monochromated Cu K α radiation on a Bruker-AXS three-circle diffractometer, equipped with a SMART Apex II CCD detector. Most single-crystal diffraction experiments were performed at 100 K under cold dry air using liquid nitrogen as the coolant. Initial space group determination was based on a matrix consisting of 120 frames. The data were corrected for Lorentz and polarization³⁶ effects and absorption using SADABS.³⁹ All structures were solved using direct methods or intrinsic phasing. Structure solution, refinement and the calculation of derived results were performed using the SHELXTL⁴⁰ package of software and ShelXle.⁴¹ Non-hydrogen atoms were refined anisotropically. All hydrogen atoms were placed in theoretical positions.

Powder X-ray Diffraction (PXRD)

PXRD data for all compounds were collected on the same instrument described above. Mulls of Paratone-N oil and the sample compounds were spread on a glass pedestal and mounted on a goniometer head.

UV/Vis Emission Spectroscopy

UV/Vis emission spectroscopy was performed by the Patterson Group at the University of Maine. Spectra were recorded with a Model Quantamaster-1046 photoluminescence spectrometer from Photon Technology International using a 75W

xenon arc lamp combined with two excitation monochromators and one emission monochromator. A photomultiplier tube at 800 V was used as the emission detector. The samples were mounted on a copper plate using non-emitting copper-dust high vacuum grease and run under vacuum using a Janis ST-100 optical cryostat.

Laser Irradiation

Laser irradiation of samples was performed with an Opolette Model 355II and UV tunable pulse laser using a Nd:YAG laser pump.

Synthesis

2.1 Bulk syntheses

2.1.1 CuSCN-sulfide complexes

(CuSCN)(Me₂S)₂, 1a. Copper(I) thiocyanate (131 mg, 1.07 mmol) was dissolved in 480 μ L of neat dimethyl sulfide in a 1 dram vial. The resulting brown solution was placed in a freezer for 3 days. The colorless crystals formed during this procedure were collected by siphoning excess ligand from the vial. The crystals were gently washed with pentane and air-dried for no more than 5 minutes. Yield 82 mg, 38.9%. Samples were immediately taken for TGA and AAS. Due to sample instability, CHN analysis was not possible. IR: 2098, 1419, 1029, 979, 771, 682. IR (cm⁻¹): 2920 (weak), 2098 (v strong), 1419, 1029, 979, 771, 682. Anal. Calcd for C₅H₁₂N₁Cu₁S₃: Cu, 25.84. Found: Cu, 25.16. TGA calcd for (CuSCN)(Me₂S): 74.7%. Found: 70.2% (20–50 °C). Calcd for CuSCN: 49.4%. Found: 53.6% (50–130 °C).

(CuSCN)(Me₂S), 1b. Copper(I) thiocyanate (121 mg, 1.00 mmol) was dissolved in 1 mL of neat dimethyl sulfide. The resulting suspension was stirred at room temperature for 1 hour in a seal vial, with the solid dissolving completely into the ligand after only a few minutes. The product was precipitated with addition of pentane. The resulting white solid was collected via filtration, and washed with pentane. Because of the ready loss of sulfide, the product was dried for no more than 5 min. prior to storage in a freezer (82

mg, 38.9% yield). Samples were immediately taken for TGA and AAS. Due to sample instability, CHN analysis was not possible. IR (cm^{-1}): 2117 (v strong), 1415, 1037, 975, 759. Anal. Calcd for $\text{C}_3\text{H}_6\text{Cu}_1\text{S}_2\text{N}_1$: Cu, 34.6. Found: Cu, 35.1. TGA calculated for CuSCN: 66.1%. Found: 67.1% (35–120 °C).

(CuSCN)(Et₂S), 2. CuSCN (96 mg, 0.798 mmol) was dissolved in 2 mL of neat diethyl sulfide. The solid dissolved within 20 minutes of stirring. The solution was stirred for 3 days. Precipitation with diethyl ether resulted in a white powder, which was isolated by filtration and washed with ether. The product was dried for no more than 5 minutes due to ready loss of ligand (103 mg, 61.6%). IR (cm^{-1}): 2970 (weak), 2169 (v strong), 1446, 1377, 1259, 974, 746. Anal. Calcd for $\text{C}_5\text{H}_{10}\text{Cu}_1\text{N}_1\text{S}_2$: Cu, 30.00. Found: Cu, 32.5. Due to sample instability, CHN was not possible. TGA calculated for (CuSCN): 58.4%. Found: 61.6% (45–95°C).

(CuSCN)(Prⁱ₂S), 3. The procedure for **2** was followed, using 119 mg (0.978 mmol) CuSCN and 2 mL of neat isopropyl sulfide. The solid did not dissolve completely, but the suspension was stirred for three days. The resulting white powder was collected via filtration through a frit and washed with diethyl ether (149 mg, 65.4%). IR (cm^{-1}): 2974 (weak), 2924 (weak), 2866 (weak), 2924 (weak), 2866 (weak), 2148, 2110 (strong), 1442, 1381, 1365, 1238, 1153, 1045, 929, 906, 883, 860, 740. Anal. Calcd for $\text{C}_7\text{H}_{14}\text{Cu}_1\text{N}_1\text{S}_2$: Cu, 26.5. Found: Cu, 26.9. Due to sample instability, CHN was not possible. TGA calculated for (CuSCN): 50.7%. Found: 54.8% (40–75°C).

(CuSCN)(THT), 4. The procedure for **2** was followed, using 126 mg (1.04 mmol) CuSCN and 2 mL of neat THT. Like **3**, the solid did not dissolve completely during the stirring. A white powder was isolated and washed with diethyl ether (156 mg, 51.7%). IR (cm^{-1}): 2951, 2125 (strong), 1435, 1253, 883, 756, 671. Anal. Calcd for $\text{C}_9\text{H}_{16}\text{Cu}_1\text{N}_1\text{S}_3$: Cu, 21.3. Found: Cu, 21.6. Due to sample instability, CHN was not possible. TGA calculated for

(CuSCN)(THT): 70.4%, Found: 72.8 (31–50°C), Calcd for CuSCN: 40.0%. Found: 43.3% (60–95°C).

2.1.2 CuSCN-diimine complexes

(CuSCN)₂(Qox), 5. CuSCN (121 mg, 1.00 mmol) was suspended in 20 mL of aqueous solution containing 1.5 mmol KSCN and 0.5 mL 17 M NH₃ under Ar purge. Qox (70 mg, 0.54 mmol) was added to the suspension, which quickly took on a red-orange color. The suspension was refluxed for 72 hours. The red-fluorescent red solid product was collected by filtration, washed with deionized water and dried under vacuum (123 mg, 65.9%). IR (cm⁻¹): 2086 (strong), 1500, 1362, 1207, 1049, 867, 764 (strong). Anal. Calcd for C₁₀H₆Cu₂N₄S₂: Cu, 34.03; C, 32.17; H, 1.62; N, 15.00. Found: Cu, 33.93; C, 31.40; H, 1.66; N, 14.45. TGA calculated for CuSCN: 65.2%. Found: 66.3% (140–190°C).

(CuSCN)(Qnz), 6. The procedure for **5** was followed using Qnz (133 mg, 1.02 mmol) in the place of Qox. A yellow solid was collected (145 mg, 56.4%). IR (cm⁻¹): 2113 (strong), 1616, 1574, 1489, 1373, 1211, 926, 791, 745, 633. Anal. Calcd for C₉H₆CuN₃S₁: Cu, 25.24; C, 42.93; H, 2.40; N, 16.69. Found: Cu, 27.08 C, 41.28; H, 2.27; N, 16.08. TGA calculated for CuSCN: 48.3%. Found: 51.9% (125–170°C)

(CuSCN)₂(Ptz), 7. The procedure for **5** was follow using Ptz (70 mg, 0.54 mmol) in place of Qox. A yellow solid was collected (87 mg, 46%). IR (cm⁻¹): 2137 (strong), 1574, 1447, 1377, 1308, 1273, 1219, 914, 741. Anal. Calcd for C₁₀H₆Cu₂N₄S₂: Cu, 34.04; C, 32.17; H, 1.62; N, 15.00. Found: 34.89; C, 31.33; H, 1.58; N, 14.51. TGA calculated for CuSCN: 65.2%. Found: 66.6% (200–250°C).

(CuSCN)₂(2-NH₂Pyz), 8. The procedure for **5** was follow using 2-NH₂Pyz (65 mg, 0.68 mmol) in place of Qox. A yellow solid was collected (106 mg, 62.7%). IR (cm⁻¹): 3418, 3317, 2102 (strong), 1616, 1593, 1528, 1435, 1215, 1029, 817, 768. Anal. Calcd for

$\text{C}_6\text{H}_5\text{Cu}_2\text{N}_5\text{S}_2$: Cu 37.56; C, 21.30; H, 1.49; N, 20.70. Found: Cu, 36.32; C, 20.41; H, 1.38; N, 19.73. TGA calculated for CuSCN : 71.8%. Found: 73.8% (190–230 °C).

(CuSCN)(2-MeOPyz), 9. 100 mg CuSCN were stirred in 500 μL neat 2-MeOPyz ligand under argon for 3 days. A yellow solid was collected on a frit and washed with ether before being dried under vacuum overnight. Yield: 154 mg, 80.8%. IR (cm^{-1}): 2123 (strong, sharp), 1587, 1529 (strong, sharp), 1471, 1438, 1398, 1311, 1284, 1195, 1145, 1060, 1014 (weak), 1004 (strong, sharp), 837, 759, 617. Anal. Calcd for $\text{C}_6\text{H}_6\text{Cu}_1\text{N}_3\text{O}_1\text{S}_1$: Cu 27.42; C 31.10; H, 2.61; N, 18.13. Found: Cu, 26.48; C, 31.12; H, 2.42; N, 17.95. TGA calculated for CuSCN : 52.4%. Found: 53.8 (75–105 °C)

(CuSCN)₂Pyz, 10. The procedure of **5** was followed using 172 mg CuSCN and 60.0 mg Pyz. A bright orange powder was obtained (yield 182 mg, 80.2%).

(CuSCN)₂(2,3-Me₂Pyz), 11. The procedure as **5** was followed using 608 mg CuSCN (5.00 mmol) and 204 mg 2,3-Me₂Pyz (2.5 mmol). An orange powder was obtained (634 mg, 72.2%).

(CuSCN)₂(2,5-Me₂Pyz), 12 The procedure as **11** was used. An orange product was obtained (708 mg, 80.6%).

(CuSCN)₂(2,6-Me₂Pyz), 13. CuSCN (126 mg, 1.03 mmol) and 2,6-dimethylpyrazine (61.2 mg, 0.56 mmol) were ground together in a Teflon container. The headspace in the container was then flushed with Ar prior to sealing in a steel jacket. The solids were heated in an oven to 40 °C overnight. After cooling, the solids were ground together once more, sealed with Ar, and heated overnight at 40 °C. The resulting bright yellow solid was collected and washed with acetone to remove unreacted ligand. The solid was then dried over vacuum (110 mg, 60.7%). IR (cm^{-1}): 2094 (strong, sharp), 1531, 1417, 1253, 1157, 1022, 867, 765, 738, 460. $\text{C}_8\text{H}_8\text{Cu}_2\text{N}_4\text{S}_2$: Cu, 36.17; C, 27.34; H, 2.29; N, 15.94. Found: Cu, 37.2; CHN analysis was not performed on this product. TGA calcd for CuSCN : 69.2. Found: 73.7 (88–100 °C).

(CuSCN)(2-NCPyz)₂, 14 CuSCN (200 mg, 1.64 mmol) and 3 mL neat 2-NCPyz were stirred in a vial under Ar at 70 °C in an oil bath for three days. The solid was then collected on a frit, washed with diethyl ether and dried over vacuum (495 mg, 90.7%).

2.1.3 CuSCN-3-substituted pyridine complexes

CuSCN(3-CIPy)₂, 15a. This compound was prepared as previously reported.¹⁰ 121 mg (1.00 mmol) CuSCN were suspended in 2 mL neat 3-CIPy in a 2-dram vial and stirred three days under argon. A highly fluorescent yellow-green powder was obtained. Yield 204 mg, 58.5%. IR (cm⁻¹): TGA calcd for (CuSCN)(3-CIPy): 67.4% Found: 70.6% (45–70 °C). TGA calcd for CuSCN: 34.9%. Found, 37.0% (70–120 °C).

CuSCN(3-CIPy), 15b. The same procedure as **13** was followed using 161 mg (1.32 mmol) CuSCN, neat 3-CIPy (164 mg, 1.45 mmol) and heating the Teflon container to 55 °C. The resulting yellow-green solid was washed with pentane and dried over vacuum (205 mg, 65.9%). IR (cm⁻¹): 2119 (strong, sharp), 1469, 1411, 1190, 1111, 1093, 1031, 908, 796, 740, 690, 634, 457. Anal Calcd for Cu₁S₁C₆N₂H₄Cl: Cu, 27.02; C, 30.64; H, 1.71; N, 11.91. Found: Cu, 27.56; C, 30.57; H, 1.63; N, 11.77.

Cu(SCN)₂(3-CIPy)₂, 15c. Crystals of **15c** grew as a byproduct from the filtrate of a heated tube reaction of CuSCN and neat 3-CIPy as dark green plates.

CuSCN(3-BrPy)₂, 16a. The procedure for **15a** was followed using 180 mg (1.48 mmol) CuSCN in 2 mL neat 3-BrPy in a 2-dram vial under argon, giving a highly fluorescent yellow-green powder (yield 555 mg, 85.7%).

CuSCN(3-IPy), 17. 243 mg (1.99 mmol) of CuSCN were ground together with 410 mg (2.00 mmol) of 3-IPy. The dry mixture was heated to 55 °C in a Teflon container overnight. After cooling the container to room temperature, the mixture was again ground and heated to 55 °C overnight. A yellow-green powder was collected and washed with acetone, then dried over vacuum (yield 523 mg, 80.0%). Anal. Calcd for C₆H₄N₂CuIS: Cu, 19.46; C, 22.06; H, 1.62; N, 8.58. Found: Cu, 19.04; C, 21.25; H, 1.10;

N, 7.95. IR (cm^{-1}): 2096 (strong), 1458, 1408, 788, 690 (strong). TGA Calcd for $(\text{CuSCN})_2(3\text{-IPy})$: 68.61%, Found: 68.62% (65–85 °C). Calcd for CuSCN: 37.23%. Found: 35.83% (90–120 °C).

2.2 Crystal growth:

1a. The crystals grown in the bulk synthesis were of sufficient quality for X-ray diffraction.

2. A vial containing 80 mg of CuSCN in 2 mL of Et_2S was stirred for 1 h. The vial was then left uncapped and undisturbed in a fume hood. Overnight evaporation of the excess neat ligand resulted in the growth of colorless blades of **2**.

3. 119 mg CuSCN with 4 mL Pr_2S were stirred in a sealed vial under Ar in an oil bath at 70 °C for 3 d. The vial was allowed to cool to room temperature and left undisturbed. Though the CuSCN did not completely dissolve in the ligand, colorless needles of **3** grew from the suspension over 3 d.

4. 119 mg CuSCN with 4 mL neat THT were stirred in a sealed vial under Ar in an oil bath at 70 °C for 3 d. CuSCN dissolved completely into the THT in this procedure. The vial was cooled to room temperature before being placed in a freezer. Colorless plates of **4** grew over 3 d.

Compounds 5, 6, 7, 8. The same procedure for the bulk synthesis of **5–8** was used, but the suspension was not stirred during the 3 d period. Crystals of each compound grew on the surface of the heated suspension and were collected by filtration on a frit.

Compound 9. CuSCN (100 mg, 0.82 mmol) was partially dissolved in 5 mL 1 M NH_3 (aq) under Ar. 2-MeOPyz (50 μL , 0.52 mmol) was dissolved in 3 mL EtOH and layered on top of the aqueous suspension and sealed in a 5 mm i.d. tube. Crystal growth became apparent after about two weeks when the small colorless blades emitted green upon exposure to UV light.

Compound 15a. CuSCN (182 mg) was suspended in a vial containing 4 mL neat 3-CIPy. The vial was sealed and heated in an oil bath at 70°C overnight without stirring. It was then cooled to room temperature by shutting off heat to the oil bath, allowing for crystals to grow. Crystals were collected on a frit and washed with diethyl ether before being dried over vacuum.

Compound 15c. The heated tube reaction of **15a** also resulted in crystals of **15c** as a byproduct, obtained by evaporating the filtrate. Crystals could also be grown by preparing a methanol solution containing copper(II) thiocyanate and 3-CIPy. Evaporation of the solvent left behind green crystals of **15c**.

Compound 16a. The same crystallization procedure as was used for **15a** was used.

2.3 Optical Memory Experiments

Optical memory experiments were based on luminescence emission measurements in the ultraviolet and visible region, taken before and after intervals of high-energy laser irradiation. Samples were initially cooled to 80 K, after which an initial spectrum was collected. Excitation wavelengths varied from sample to sample. After the initial scan, each sample was irradiated for 5-min. intervals, up to a total of 20 min. This laser wavelength was tuned from 240–266 nm. A new spectrum was obtained after each interval. To measure emission intensity recoveries, each sample was warmed to 298 K, and then cooled to 80 K once more. A final scan was performed and compared with the initial non-irradiated spectrum. Samples with positive results after one cycle were subjected to up to three write/read/erase cycles to gauge durability.

Results and Discussion

4.1 Synthesis and Characterization

Number	Compound	Network type	Space group
1a	(CuSCN)(Me ₂ S) ₂	1-D chain	<i>P2₁/c</i>
1b	(CuSCN)(Me ₂ S)	n/a	n/a
2	(CuSCN)(Et ₂ S)	1-D ladder	<i>P2₁/n</i>
3	(CuSCN)(Pr ⁱ ₂ S)	1-D ladder	<i>P2₁/n</i>
4	(CuSCN)(THT)	1-D chain	<i>P2₁</i>
5	(CuSCN) ₂ Qox	2-D bridged ladders	<i>P2₁/n</i>
6	(CuSCN)Qnz	2-D <i>trans</i> -fused sheet	<i>Cc</i>
7	(CuSCN) ₂ Ptz	2-D <i>cis/trans</i> sheet	<i>Pbca</i>
8	(CuSCN) ₂ (2-NH ₂ Pyz)	2-D bridged ladders	<i>P-1</i>
9	(CuSCN)(2-MeOPyz)	2-D <i>cis</i> -fused sheet	<i>Pnnm</i>
10	(CuSCN) ₂ Pyz	3-D <i>trans</i> -fused sheets	<i>P2₁/c</i>
11	(CuSCN) ₂ (2,3-Me ₂ Pyz)	3-D dimer chains	<i>C2/c</i>
12	(CuSCN) ₂ (2,5-Me ₂ Pyz)	3-D <i>trans</i> -fused sheets	<i>P2₁/n</i>
13	(CuSCN) ₂ (2,6-Me ₂ Pyz)	n/a	n/a
14	(CuSCN)(2-NCPyz) ₂	1-D chain	<i>Cm</i>
15a	(CuSCN)(3-ClPy) ₂	1-D chains	<i>Pc</i>
15b	(CuSCN)(3-ClPy)	2-D sheets	<i>P2₁/n</i>
15c	Cu(SCN) ₂ (3-ClPy) ₄	monomer	<i>C2/c</i>
16	(CuSCN)(3-BrPy) ₂	1-D chains	<i>Pc</i>
17	(CuSCN)(3-IPy)	n/a	n/a

Table 1. Summary of compounds.

4.1.1 Synthesis of CuSCN-alkyl sulfide compounds

All five compounds containing L = Me₂S, Et₂S, Prⁱ₂S or THT were generated readily by stirring CuSCN in the respective neat ligand. This method was previously used in preparing monodentate aromatic amine compounds.¹⁰ In the case of **1a**, **1b**, and **2**, the reagents formed a solution within minutes; both **1a** and **1b** were collected from a brown solution, while **2** formed a completely colorless solution in excess ligand. Agitation with a non-polar organic solvent, in this case pentane or ether, resulted in

precipitation of the compounds from solution. The off-white CuSCN did not completely dissolve in either isopropyl sulfide or THT. However, stirring the solid in the neat ligand over several days effectively converted the off-white starting material into the pure white products. Notably, yields for the less soluble **3** and **4** were higher than those of **1a**, **1b** or **2**. The reaction of CuSCN in neat Me₂S resulted in two different products, depending upon the procedure used. Cooling a highly concentrated solution of CuSCN allowed for colorless blocks to crystallize; these were found to be the 1:2 product (CuSCN)(Me₂S)₂ by X-ray diffraction, TGA, and atomic absorption analysis. Precipitating solid from a more dilute solution using pentane gave the 1:1 product (CuSCN)(Me₂S). Figure 12 shows the powder diffraction patterns of both compounds; they are distinct from each other and from that of CuSCN. Only one product was obtained from each of the other three CuSCN-sulfide reactions.

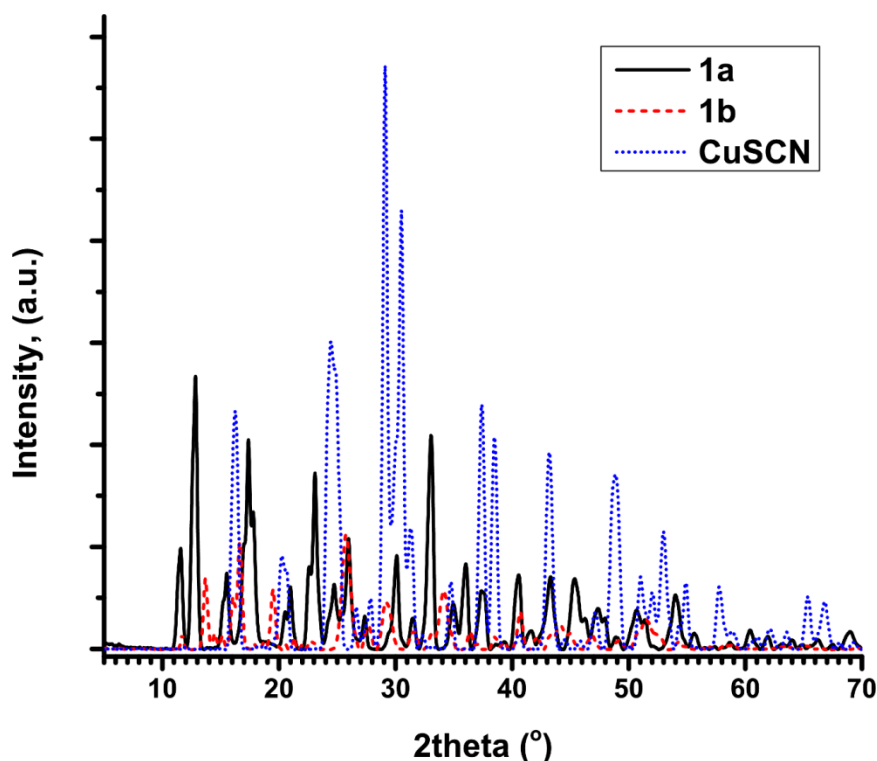


Figure 12: PXRD patterns of **1a**, **1b** and CuSCN.

All synthesized compounds of CuSCN and alkyl sulfides were found to be thermally unstable at room temperature. This was made apparent by comparison of TGA traces of samples left to air-dry for short and long periods of time at ambient temperature. Samples dried for up to five minutes gave traces which matched the expected mass losses; samples dried for extended periods of time showed smaller mass losses and a high residual CuSCN mass after the ligand loss. Traces for the five compounds are shown in Figure 13. As a result of this instability, samples for TGA, PXRD and Cu-AAS needed to be prepared immediately after a very brief period of air-drying. Ligand loss took place from ambient temperature ($\sim 22\text{ }^{\circ}\text{C}$) to $135\text{ }^{\circ}\text{C}$, by which point all compounds had decomposed to CuSCN, which itself decomposed above $400\text{ }^{\circ}\text{C}$. Compounds could be preserved by storage in sealed vials at $5\text{ }^{\circ}\text{C}$ for periods of days or weeks, after which ligand loss became apparent from TGA traces.

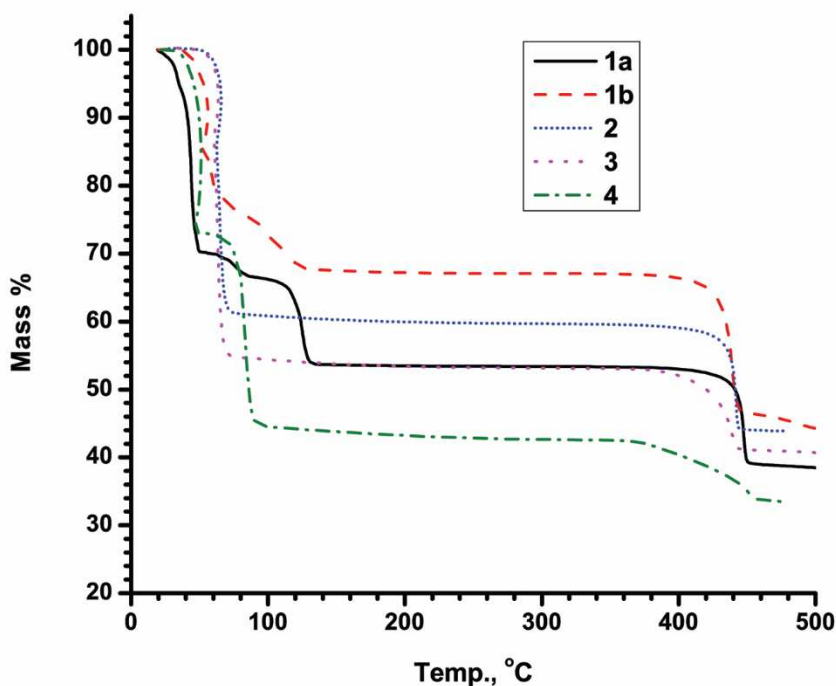


Figure 13: Thermogravimetric analysis results for alkyl sulfide compounds.

4.1.2 Synthesis of CuSCN-diimine compounds

Eight of the ten CuSCN-diimine networks were successfully synthesized by refluxing an aqueous suspension containing CuSCN, the ligand, KSCN and ammonia. KSCN and ammonia, acting as mineralizing and phase-transfer agents respectively, were found to be crucial in ensuring complete conversion of the sparingly soluble CuSCN to the products. Solids obtained from reactions lacking either reagent, and for reactions run for less than 72 hours, were found to have higher copper content and smaller mass losses by TGA trace than anticipated based on complete conversion. Peaks corresponding to CuSCN were also found in PXRD patterns of samples containing unreacted starting material. A slight stoichiometric excess of ligand was used to further promote formation of the desired products. Although suspensions of each of the six compounds took on the color of the corresponding product within moments after addition of the ligand, prolonged reflux periods were required to complete the reaction. TGA traces of the six new compounds can be found in Figure 14. The traces clearly demonstrate that the monodentate, 1:1 compounds (**6** and **9**) lose ligand at markedly lower temperatures than those for the bidentate complexes. The limited solubility of CuSCN and the resulting metal-organic networks proved advantageous for crystal growth. Single crystals suitable for X-ray diffraction were obtained from unstirred refluxing mixtures of the same reaction mixture over the same period of time.

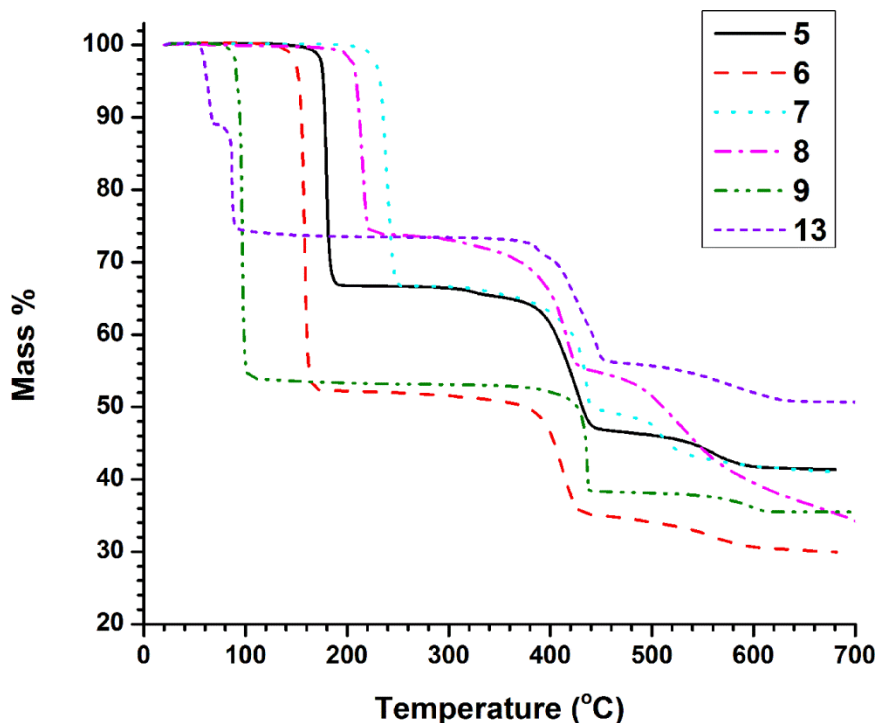


Figure 14: Thermogravimetric analysis results for **5**, **6**, **7**, **8**, **9** and **13**.

Compound **9** was produced in a manner similar to that used for the CuSCN-alkyl sulfide networks. CuSCN was stirred as a solid in neat 2-MeOPyz for several days. Pure samples of **9** could not be obtained using the aqueous reflux method, thus necessitating the need for a direct reaction. As with the above eight compounds, the suspension rapidly took on the green-yellow color of the product, but the prolonged reaction time ensured complete conversion of CuSCN. Crystals of **9** were obtained by layering an ethanol solution of 2-MeOPyz over top of CuSCN in aqueous ammonia. Growth of these crystals became apparent after exposing the solid in the crystallization tube to 365 nm UV light, causing the colorless crystals to emit green light. Compound **14** was obtained in a similar manner as **9**, but stirred at 70 °C.

The final new CuSCN-diimine compound, **13**, was prepared by means of a solid-state reaction in sealed vessels at the rather modest temperature of 40 °C. Attempts to produce the compound using the aqueous ammonia/KSCN method proved unsuccessful. Grinding the solid starting materials at room temperature resulted in

impure samples of **13**; addition of a moderate amount of heat enabled the ligand to melt and react more readily with CuSCN.

4.1.3 Synthesis of CuSCN 3-XPy compounds

Three of the CuSCN 3-XPy compounds (where X = Cl, Br, I), **15a**, **15b**, and **16**, have been previously reported.¹⁰ Stirring CuSCN and neat 3-ClPy or 3-BrPy under argon at ambient temperature for 3 days gave pure powder samples of the 1:2 compounds **15a** and **16**. Unstirred heated sealed tube reactions using these same reagents under argon at 70 °C enabled growth of single crystals of each network. **15c** was obtained as a byproduct of the tube containing **15a** both from the reaction vessel and from evaporation of the filtrate. The 1:1 compound **15b** was formed from a stoichiometrically controlled reaction resembling that in the procedure used for **13**. Solid CuSCN and neat 3-ClPy were ground together in a Teflon container, sealed with argon, and placed in an oven at 55 °C. After 24 hours, the vessel was cooled to room temperature. The solid was ground before being sealed with argon and heated to 55 °C once more. The green-yellow product was washed and collected thereafter. TGA and PXRD confirmed that this procedure resulted in pure **15b**. Surprisingly, the 1:1 network (CuSCN)(3-BrPy) was not obtained from this procedure when using 3-BrPy, instead affording a mix of the 1:2 product and CuSCN. Finally, samples of **17** were synthesized using the same procedure as was used for **15b**. Crystals could not be obtained even by slow cooling of the hot vessel.

4.2.1 Structures of CuSCN-alkyl sulfides

Crystal structures were obtained for four of the five compounds prepared. The resulting structures fall under two of the common categories outlined in Chart 1: 1-D chains and 1-D ladders. In all cases, alkyl sulfide ligands acted as monodentate ligands. This result stands in contrast with a number of known CuCl, CuBr, CuI and CuCN complexes with bridging Me₂S and THT ligands.²²

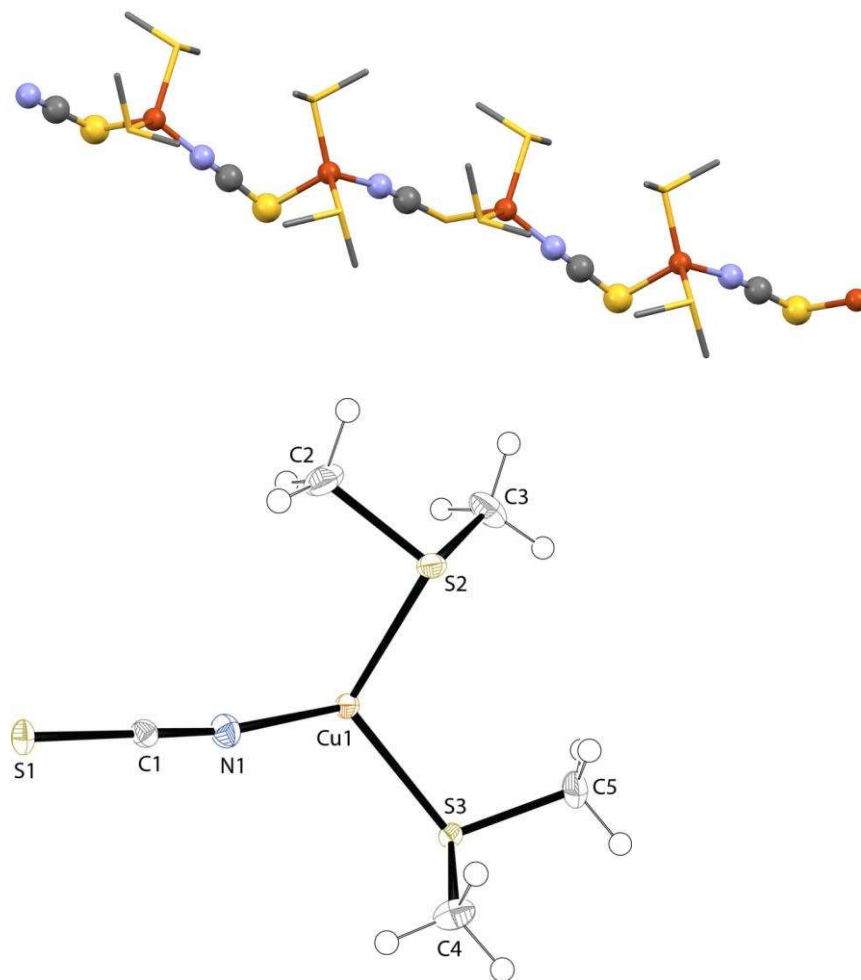


Figure 15. Structural diagrams of **1a**. Top, networking of **1a**, viewed down the *b*-axis. CuSCN are shown as ball and sticks; ligand molecules shown as wire frames. Bottom, thermal ellipsoid rendering of the asymmetric unit. All thermal ellipsoid renderings at 30% probability unless otherwise noted.

Colorless blocks of **1a** were solved in the centrosymmetric monoclinic space group $P2_1/c$. Structural diagrams are shown in Figure 15. The structure is a Type A, 1-D zig-zag chain of CuSCN, with the coordination sphere of Cu centers completed by two monodentate Me₂S ligands. The chain propagates along the *c*-axis, and has zigzag angles S1-Cu1-S1 = 106.74(5)° and C1-S1-Cu1 = 96.41(7)°. The angles around the Cu atom range from 104.33(2)° to 117.24(5)°. Interestingly, both Cu–S bonds associated with the sulfide molecules (Cu–S2 = 2.3456(5), Cu–S3 = 2.2869(4) Å) are shorter than

that of the thiocyanate ($\text{Cu}-\text{S1} = 2.3783(6) \text{ \AA}$). The chain is not perfectly straight, as the CuSCN lies in two slightly displaced positions, resulting in a $\text{Cu1}\cdots\text{Cu1}\cdots\text{Cu1}$ angle of 173.64° and a $\text{S1}\cdots\text{Cu1}\cdots\text{Cu1}\cdots\text{S1}$ dihedral angle of 27.06° . There are no apparent interactions between chains.

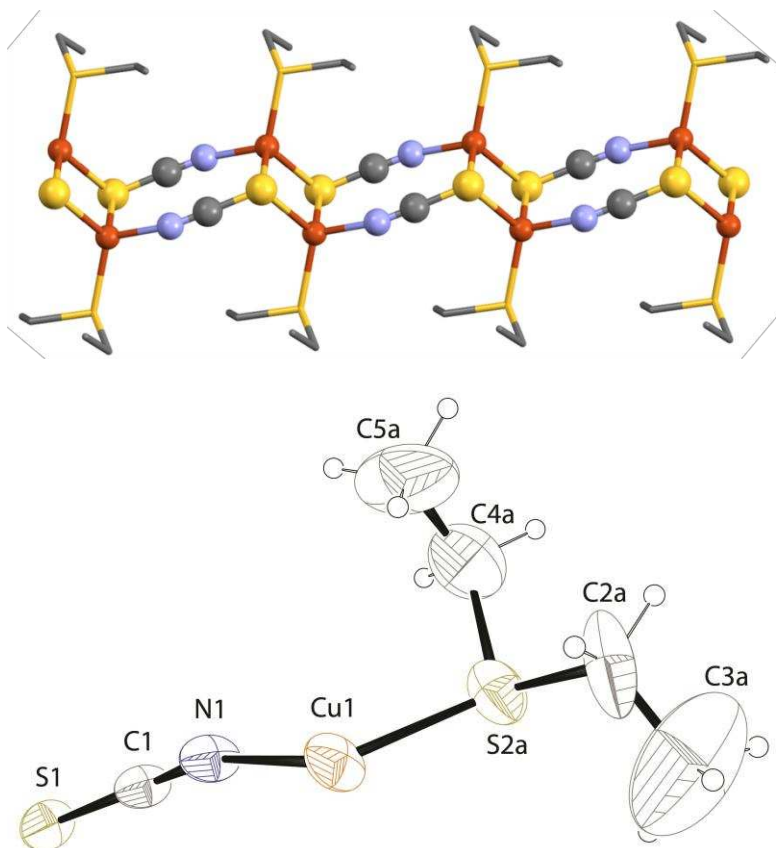


Figure 16. Structural diagrams of **2**. Top, networking of **2** viewed along the c -axis. Hydrogen atoms and disordered ligand positions are omitted for clarity. Bottom, thermal ellipsoid rendering. Ligand disorder has been omitted.

Compound **2** crystallized as colorless needles that solved in the centrosymmetric monoclinic space group $P2_1/n$. The networking of **2** is shown in the top diagram of Figure 16 above, while the asymmetric unit $(\text{CuSCN})(\text{Et}_2\text{S})$ is shown in the bottom as a thermal ellipsoid rendering. Because crystals of **2** underwent a destructive phase change upon modest reduction in temperature, data were collected at 298 K. The structure

contains significant disorder; Et₂S molecules are modeled over two positions but, even so, continue to show large thermal ellipsoids (see Figures 16 and 17).

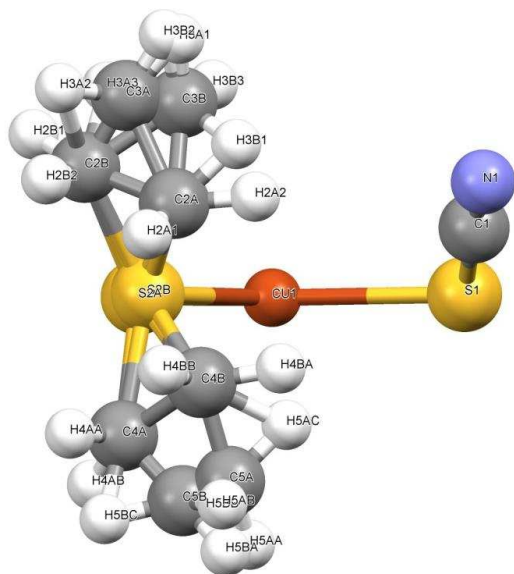


Figure 17. Asymmetric unit of **2** showing disorder of the ethyl sulfide molecule.

The networking of **2** consists of a 1-D Type B ladder, formed by crosslinking of antiparallel chains of CuSCN by μ_3 -S bridging. This type of bridging results in two ring motifs: Cu₂S₂ rhomboid dimers and Cu₂(SCN)₂ rings, which alternate and share a CuS edge. The ladders propagate along the crystallographic *a*-axis. One Et₂S ligand molecule completes the coordination sphere of the Cu centers. The Cu1...Cu1 distance in the rhomboid dimers is 2.8893(7) Å, just outside the van der Waals radius sum of copper (2.8 Å). This close distance results in a shortened Cu–S–Cu angle of 72.74(3)°. Distances between Cu and thiocyanate S (Cu–S = 2.368(1), 2.500(1) Å) are slightly longer than those between Cu and S of the aliphatic ligand (Cu–S2A = 2.227(5), Cu–S2B = 2.294(9) Å). There appear to be no interactions between adjacent ladders, which are rotated 90° with respect to one another.

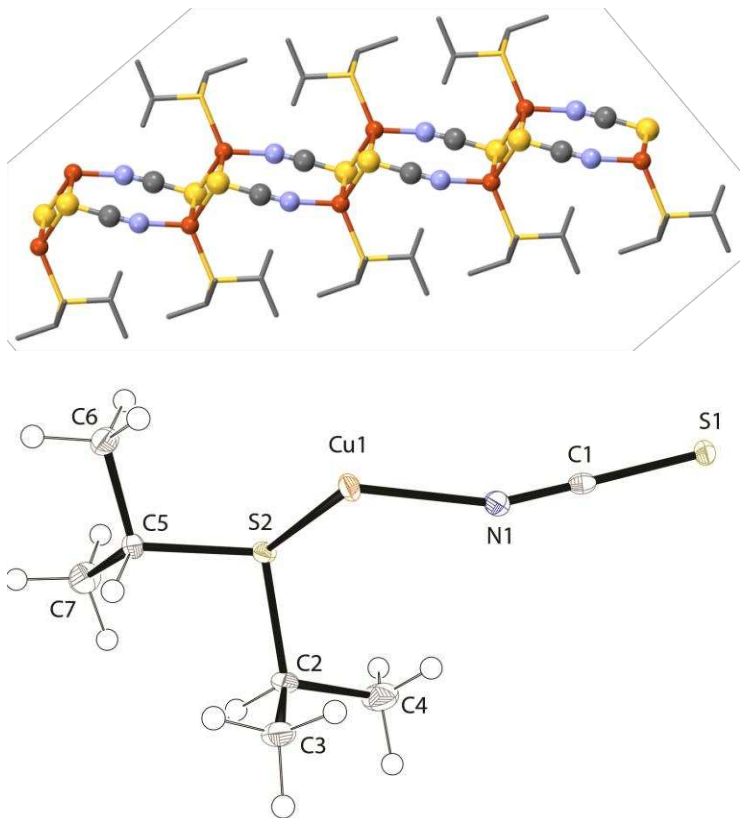


Figure 18: Top, ladder of **3** viewed down the *c*-axis. Hydrogen atoms are omitted. Bottom, asymmetric unit of **3** shown as a thermal ellipsoid rendering.

Compound **3** crystallized as thin colorless needles that solved in the centrosymmetric monoclinic space group $P2_1/n$. Like **2**, it formed a Type B ladder network, which extends along the crystallographic *a*-axis. Unlike **2**, the crystals did not undergo destructive phase changes at reduced temperatures, enabling data collection at 100 K. The structure contained no disorder and showed much smaller thermal factors than were seen in **2** (see bottom of Figure 18). Another difference between the two structures is the Cu1 \cdots Cu1 distance and the resulting rhomboid dimer angles. This distance in **3** was 3.1662(5) Å, well outside the van der Waals radius sum of Cu, and the Cu–S–Cu angle was widened to 81.08(2)°. This inverse relationship between Cu \cdots Cu distance and Cu–E–Cu angle, where E = S, Cl, Br or I, is also apparent in several reported structures,^{33,34} including (CuI)₂Qox, which contains both long and short Cu \cdots Cu

distances in the ladder motif.³³ The shorter bond distances correspond to smaller Cu–S–Cu angles. Like **1a** and **2**, the bond distances between copper and the thiocyanate sulfur atoms (2.4816(6) and 2.3883(6) Å) are longer than those of copper and the ligand sulfur atom (2.2740(5) Å). The ladders do not appear to have any interactions with one another.

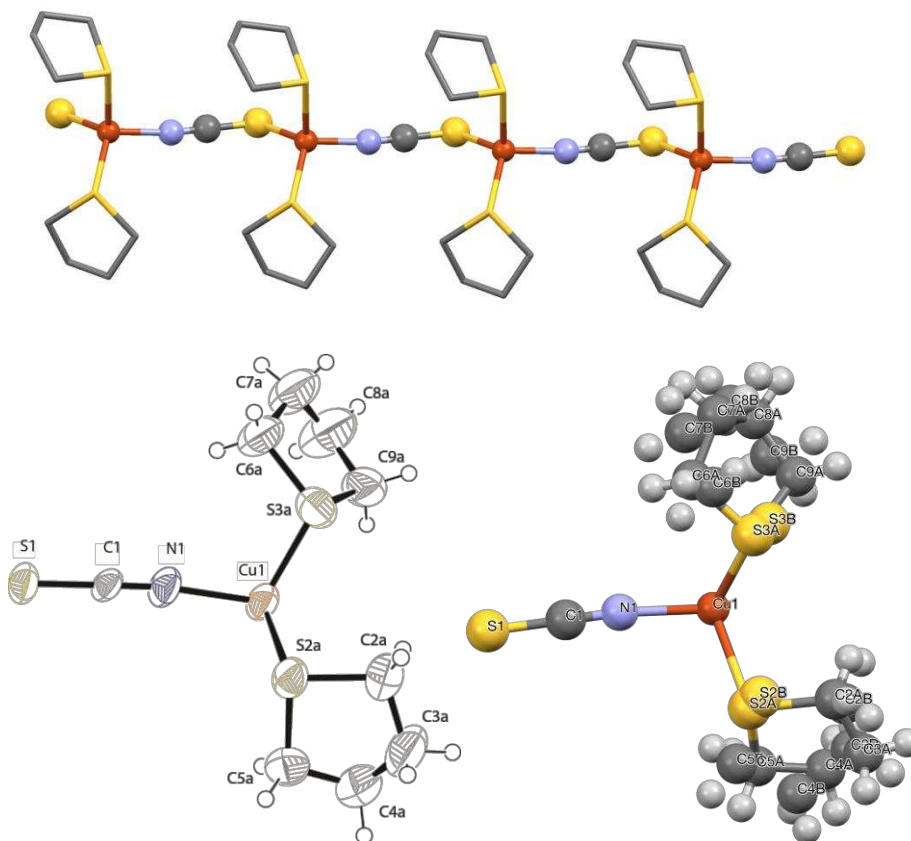


Figure 19. Top, chain of **4** viewed down the *a*-axis. Hydrogen atoms and disorder have been omitted. Bottom left, thermal ellipsoid rendering. Bottom right, asymmetric unit showing disorder of THT molecule.

Compound **4** crystallized as thin, colorless and transparent plates, solving in the non-centrosymmetric monoclinic space group $P2_1$. Like those of **2**, the crystals of **4** underwent a destructive phase change upon a modest reduction in temperature, necessitating data collection at 298 K. Both ligand molecules were disordered and modeled over two positions, shown in the center diagram of Figure 19. Also like **2**, the

ligand atoms show somewhat large thermal ellipsoids. The structure consists of a Type A 1-D CuSCN chain, with each copper atom capped by two THT ligands. The top diagram in Figure 19 shows a single chain of the compound, which resembles compound **1a**. The chain propagates along the crystallographic *a*-axis. Angles around Cu are close to tetrahedral, ranging from 103.5(3)–117.7(6)°, including the zigzag angle, N1–Cu1–S1, of 110.06(15)°. Unlike **1a–3**, the bond distance between the copper and thiocyanate sulfur (2.344(2) Å) falls within the range of Cu–S_{THT} distances: Cu–S2A = 2.40(2), Cu–S2B = 2.35(2) Cu–S3A = 2.19(2), Cu–S3B = 2.366(6) Å. No interactions were found between chains of **4**.

4.2.2 Structure of CuSCN-diimine networks

Structures were solved for five of the six new CuSCN-diimine compounds. Once again, all could be categorized under one of the common CuSCN networking motifs: two 2-D Type B ladders and three 2-D Type C sheets were found. No unexpected solid-state phase changes were observed amongst these compounds; all data were collected at 100 K. Notably, Qox, Qnz, and Ptz demonstrated completely different networking behavior in contrast with their single-ring analogs Pyz, Pym and Pdz respectively.

Compound **5** crystallized as long red needles that solved in centrosymmetric monoclinic space group $P2_1/n$. Network diagrams are shown in Figure 20. The asymmetric unit consists of (CuSCN)₂(Qox). The structure consists of a 2-D Type B ladder of CuSCN, much like **2** and **3**, but the Qox ligand bridges between ladders, resulting in a sheet. The Cu–NCS distances of 1.975(3) and 1.983(3) Å are significantly shorter than the Cu–N_{aromatic} distances of 2.019(3) and 2.032(3) Å, a pattern expected amongst all CuSCN-diimine compounds. The arrangement of **5** bears some resemblance to (CuI)₂Qox.³³ In both networks, the diimine ring of the Qox ligand points “up” between one pair of CuSCN ladders and “down” between the next pair. The Qox ligands appear to show no intermolecular interactions, because the long 4.14 Å distance

between the closest centroids rules out π -stacking between aromatic rings. Adjacent pairs of ladders are related by mirror symmetry. When viewed down the *a*-axis (bottom of Figure 20), a square-wave pattern can be seen, formed by the CuSCN ladders and the Qox ligand. As with **2**, $(\text{CuI})_2(\text{Qox})$, and other reported CuSCN ladder networks,³⁴ the short Cu...Cu distance of 2.7305(6) Å across the Cu_2S_2 dimer corresponds with relatively acute angles about sulfur of 67.79(3) and 70.17(3)°.

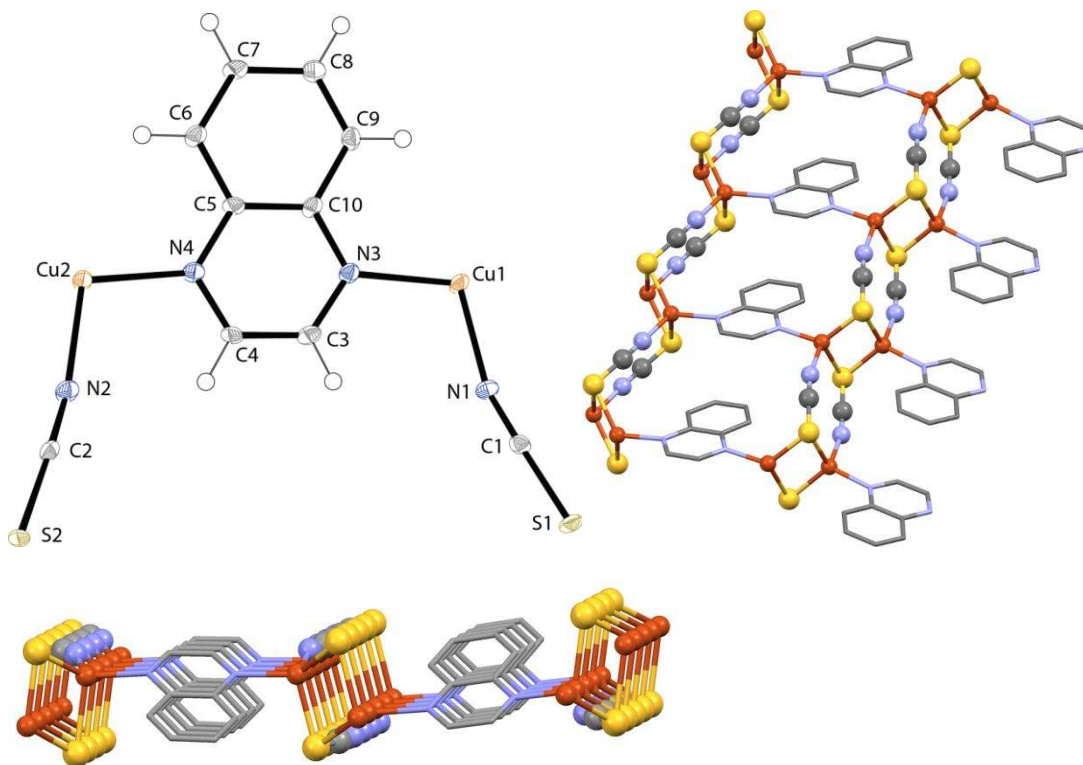


[Figure 20]. Top left, thermal ellipsoid rendering of **5**. Top right, networking of **5** viewed along the *c*-axis. Hydrogen atoms have been omitted for clarity. Bottom: view along the *a*-axis.

Compound **6** crystallized as small yellow plates that solved in the non-centrosymmetric monoclinic space group *Cc*. The structure is a Type C 2-D sheet of *trans*-fused hexagonal $\text{Cu}_3(\text{SCN})_2\text{S}$ rings, capped on one face of the sheet by monodentate Qnz ligands, which coordinate to Cu exclusively through the 1-position

nitrogen atom. Structural diagrams are shown in Figure 21. This arrangement results in some similarity to the parent CuSCN network, with the capped sheet resembling a single layer of a β -phase 3-D sheet. The network is most similar to (CuSCN)(5-BrPy), another 1:1 *trans*-fused Type C network.¹³ The sheets in **6** run parallel to the crystallographic *b,c* plane. Another motif, a (CuS) $_{\infty}$ chain, propagates parallel to the *b*-axis. Each Cu atom is coordinated with two thiocyanate sulfur atoms, one thiocyanate nitrogen, and one Qnz nitrogen. The angles about Cu centers are rough tetrahedral and range from 106.30(19)–112.4(3)°. The Qnz along a single (CuS) $_{\infty}$ chain are canted in the same orientation and are π -stacked with identical centroid-centroid distances of 3.764 Å between adjacent carbocyclic rings and between adjacent heterocyclic rings. The rings bound to the next (CuS) $_{\infty}$ are canted at a slightly different angle, but are likewise π -stacked. As a result, the Qnz cant angle alternates between adjacent (CuS) $_{\infty}$ chains, with an inter-planar angle of 44.62°. All the sheets are identically aligned, such that the carbocyclic Qnz rings lie relatively close to the undecorated side of the adjacent sheet. This results in several close interactions between ring hydrogens and thiocyanate: H6 \cdots C1 = 3.025 Å, H6 \cdots S1 = 2.864 Å, H5 \cdots N1 = 3.154 Å, H5 \cdots C1 = 3.337 Å. The bottom diagram of Figure D2 shows these potential bonding interactions. Table 2 summarizes the distances between the atoms.

Atom 1	Atom 2	Distance (Å)	Atom 1	Atom 2	Distance (Å)
H2	C1(SCN)	2.666	H7	C4(Qnz)	2.839
H5	S1(SCN)	2.921	H7	N3(Qnz)	2.709
H6	S1(SCN)	2.863			

Table 2. Distances of potential bonding interactions in **6**.

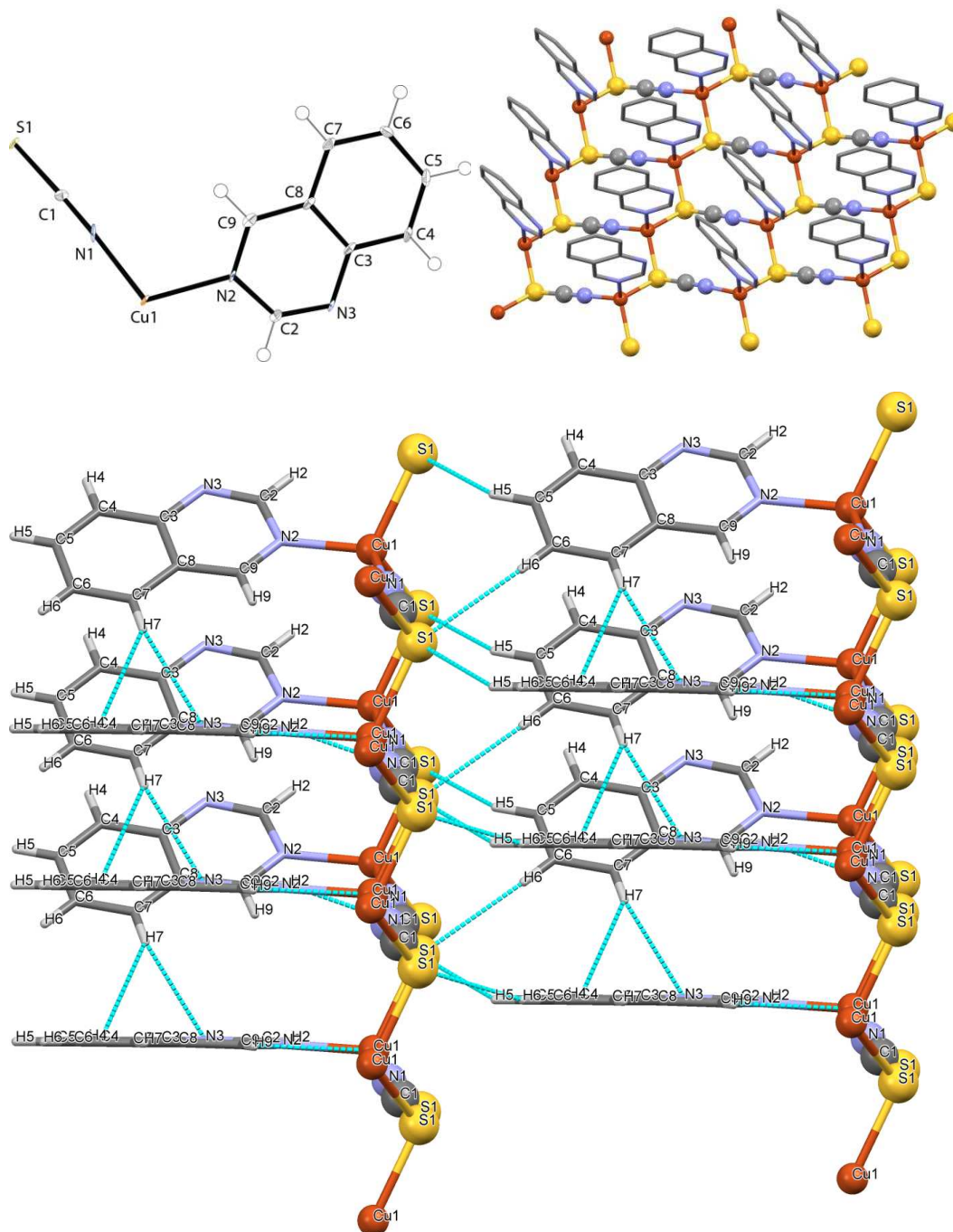


Figure 21: Top left, thermal ellipsoid rendering of **6**. Top right, networking of **6**. Hydrogen atoms are omitted. Bottom, diagram showing interactions between hydrogens and thiocyanate or Qnz rings.

Compound **7** crystallized as yellow plates, solving in the centrosymmetric orthorhombic space group *Pbcn*. The asymmetric unit is shown in Figure 22. Networking

diagrams are shown in Figure 23. Like **6**, the network can be classified as a 2-D, Type C sheet of CuSCN; however, Ptz does not act as a monodentate ligand, nor as a bridging ligand between sheets, but instead bridges between Cu atoms of a single sheet.

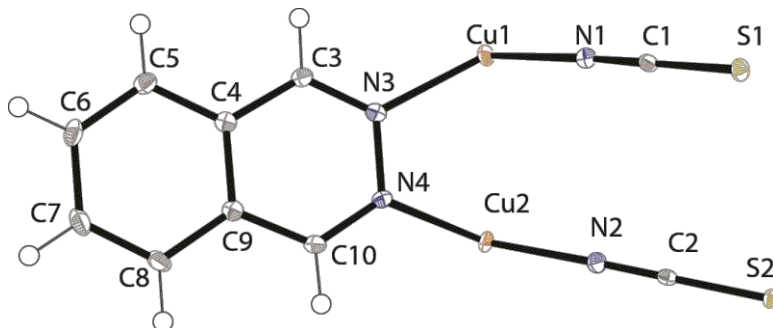


Figure 22. Asymmetric unit of **7** shown as a thermal ellipsoid rendering.

Thus, in addition to the hexagonal rings and $(\text{CuS})_\infty$ chain motifs, each Ptz produces a five-membered $\text{Cu}_2\text{N}_2\text{S}$ ring. This type of bridging can be referred to as “stapling,” and results in a number of remarkable structural characteristics in **7**. First, the Ptz ligand forces much closer $\text{Cu}\cdots\text{Cu}$ distances of 3.042 Å when compared with unstapled pairs of Cu along a CuS chain ($\text{Cu}\cdots\text{Cu} = 3.889$ Å). Significant strain is applied to the bond angles around Cu and S of stapled rings; the angles about Cu range from $93.58(4)^\circ$ to $134.53(7)^\circ$, while the stapled $\text{Cu}-\text{S}-\text{Cu}$ bond angle is $77.083(16)^\circ$. For comparison, unstapled $\text{Cu}-\text{S}-\text{Cu}$ measures at $109.84(2)^\circ$. The hexagonal CuSCN sheets are likewise strained by the stapling effect; half of the rings are in the *trans* chair conformation, while the other half are in a twist boat conformation. This differs significantly from the normally all-*cis* or all-*trans* conformation of the sheets in networks such as **6** or **9**. While only moderate distortion is apparent along a CuSCN chain, the stapling of Ptz between Cu atoms along a $(\text{CuS})_\infty$ chain causes significant distortion to the typical zig-zag angles.

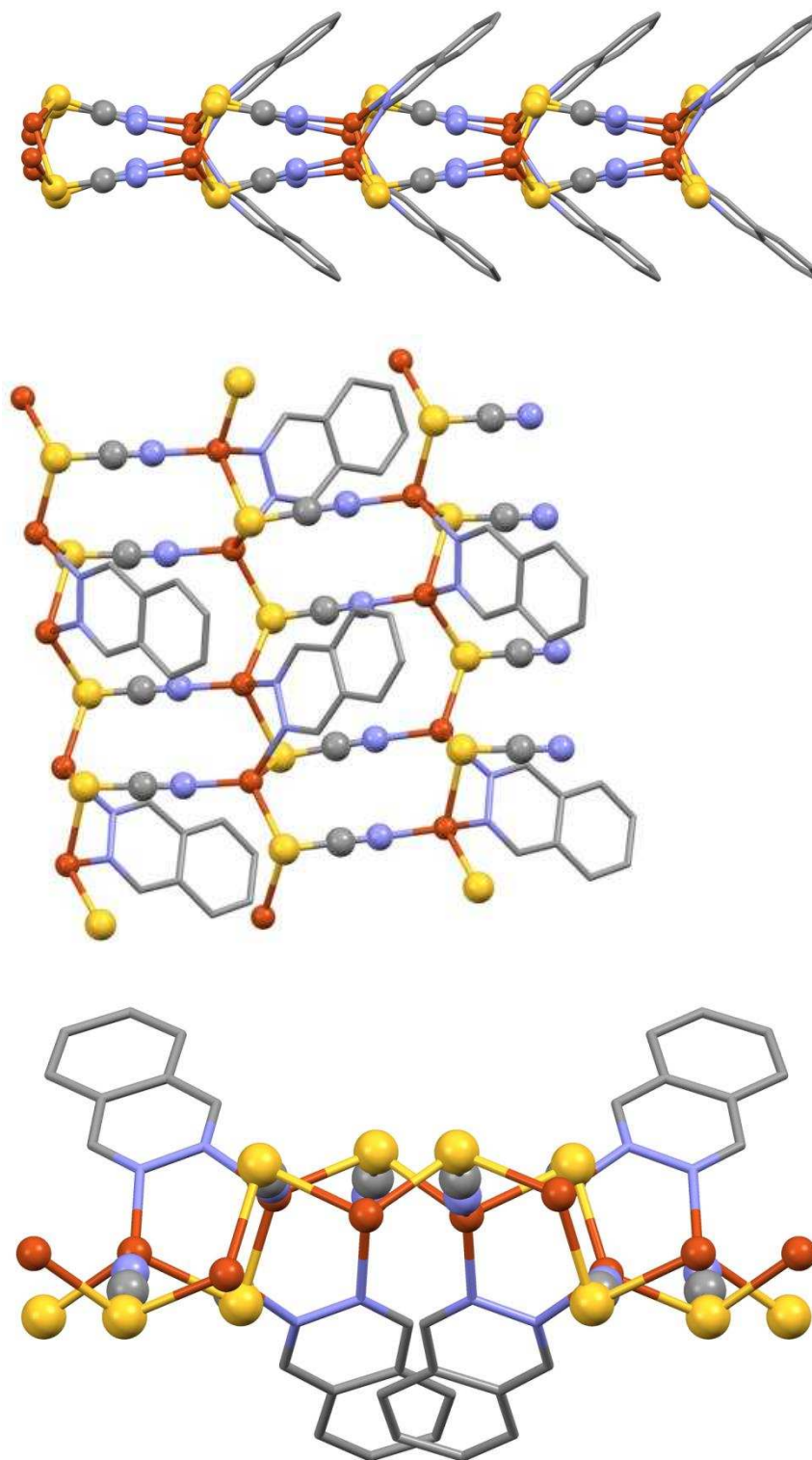


Figure 23. Networking diagrams of **7**. Top: view along the *a*-axis. Center: view along the *c*-axis. Bottom: view of square-wave pattern along the *b*-axis.

Along a $(\text{CuS})_\infty$ chain, Ptz ligands alternate between faces of the sheet, producing a roughly square wave pattern of Cu–S–Cu–S. There appear to be no interactions between separate sheets, and no π -stacking between Ptz molecules. There are two orientations of the Ptz group, their ring planes lying at angles of 15.9° to one another. The Ptz planes are found to lie at angles of 50.5° and 51.0° with respect to the CuSCN sheet plane (calculated using the nearly-parallel CuSCN units). Lastly, the unique bridging behavior of Ptz is remarkable in relation to the monodentate binding behavior of its single-ring analog Pdz, which forms the known network $(\text{CuSCN})(\text{Pdz})$, a *cis*-fused 2-D sheet similar to **9** containing monodentate Pdz ligands without significant angular or bonding length distortions.²¹

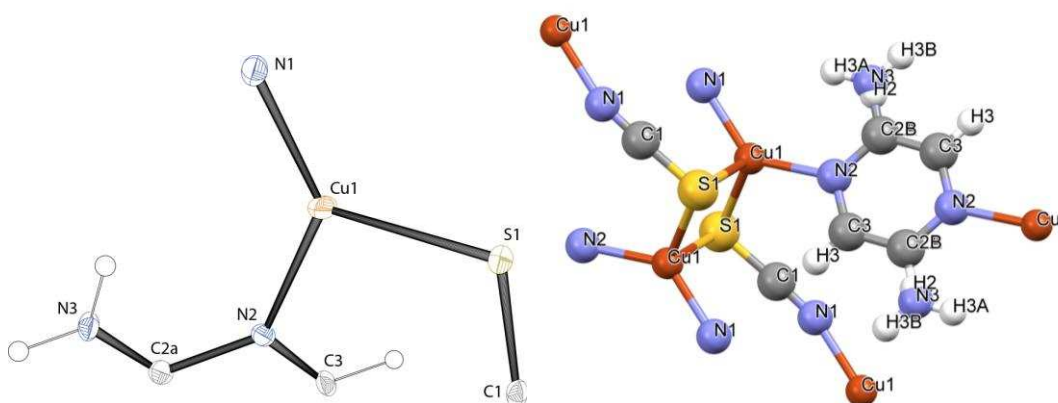


Figure 24. Left, asymmetric unit of **8** as a thermal ellipsoid rendering. Right, diagram showing disorder in the 2-NH₂Pyz molecule.

Compound **8** crystallized as orange blocks that solved in the centrosymmetric triclinic space group $P\bar{1}$. The asymmetric unit $(\text{CuSCN})(2\text{-NH}_2\text{Pyz})_{0.5}$ is shown in Figure 24. Network diagrams are shown in Figure 25. The 2-NH₂Pyz ligand is centered on an inversion center. Thus, the atoms are only half-independent, and the substituent amine group is disordered over two positions. Like **5**, the network is comprised of 2-D Type B bridged CuSCN ladders, which in this case propagate along the *a*-axis. The arrangement of the ladders, however, is significantly different. The ladders themselves

are related by inversion rather than the mirror symmetry seen in **5**. This causes adjacent zig-zag ladders to be in phase with each other, resembling the known structure $(\text{CuSCN})_2(2\text{-MePyz})$.¹³ The Cu_2S_2 dimers are oriented identically in adjacent ladders. Linking of the ladders by 2- NH_2Pyz occurs in a direction parallel to the a,c -axis bisector. Also unlike **5**, the $\text{Cu}\cdots\text{Cu}$ separation of 3.0032(10) Å in the Cu_2S_2 dimers is too large to be considered bonding, giving a less acute Cu–S–Cu angle of 72.89(2)°.

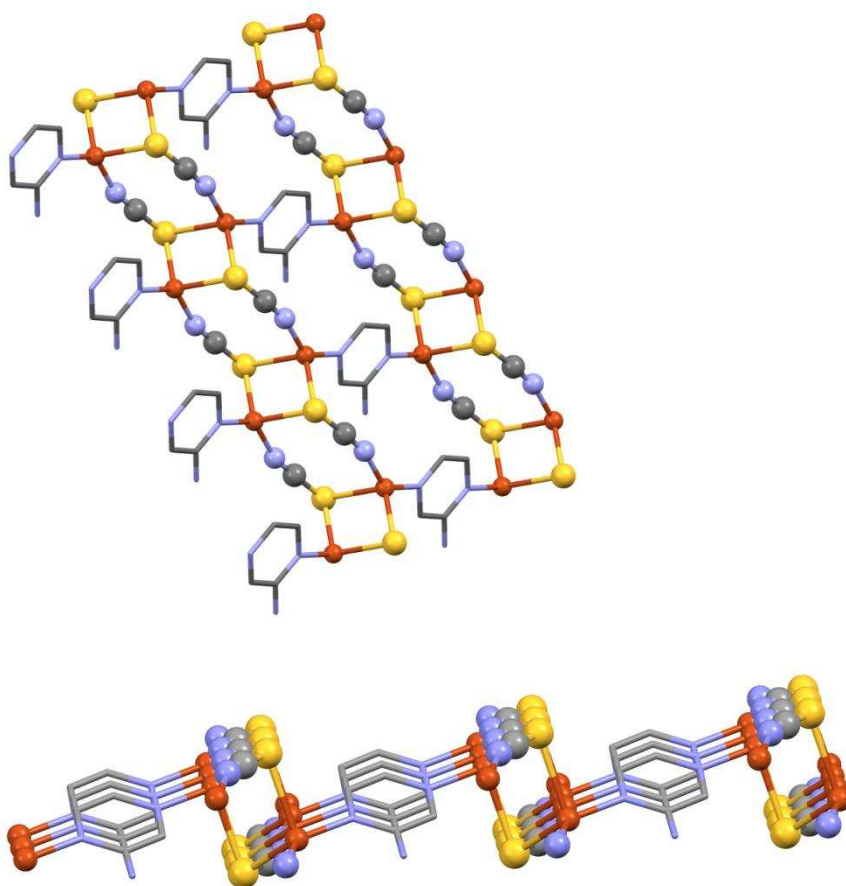


Figure 25. Networking views of **8**. Top: view along b -axis. Center: view along a -axis. Bottom: view of zig-zag pattern at an oblique angle.

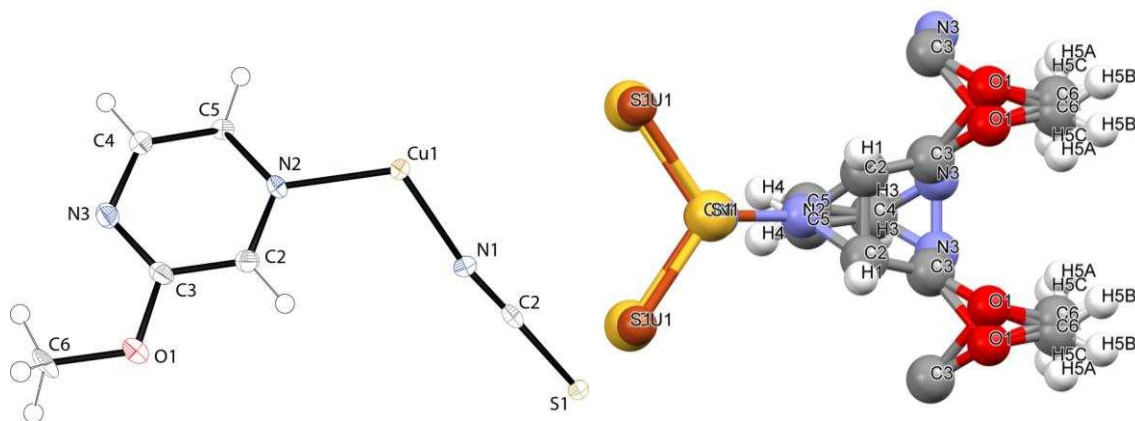


Figure 26. Left, asymmetric unit of **5** shown as a thermal ellipsoid rendering. Right, diagram showing disorder of 2-MeOPyz molecule

The final diimine structure, compound **9**, crystallized as small, colorless, green-luminescent blades, solving in the centrosymmetric orthorhombic space group $Pnmm$. The networking structure consists of Type C sheets with *cis* ring fusions. Networking of **9** is shown in Figure 27. Like Qnz in **6**, 2-MeOPyz acts as a monodentate ligand. Unlike **6**, 2-MeOPyz is present on both faces of the sheet, as is seen in $(\text{CuSCN})(2\text{-Me-3-EtPyz})$ and $(\text{CuSCN})(\text{PdZ})$.^{17,21} The *cis*-fusion of the sheets, which run parallel to the a,c plane, enables decoration of the sheet on both faces. Due to the crystallographic mirror planes in the unit cell, all atoms have only 50% occupancy. All CuSCN atoms, in addition to N1 (coordinated to Cu) and C3 (*meta* to N1) of the 2-MeOPyz ligand, lie directly on a mirror plane. The remaining atoms C1, C2, C4, N2, O1, and C5 are slightly displaced to either side of a mirror plane, resulting in two-site disorder. This is shown in the left diagram of Figure 26. There is no evidence of interactions between the sheets, or of π -stacking in the structure.

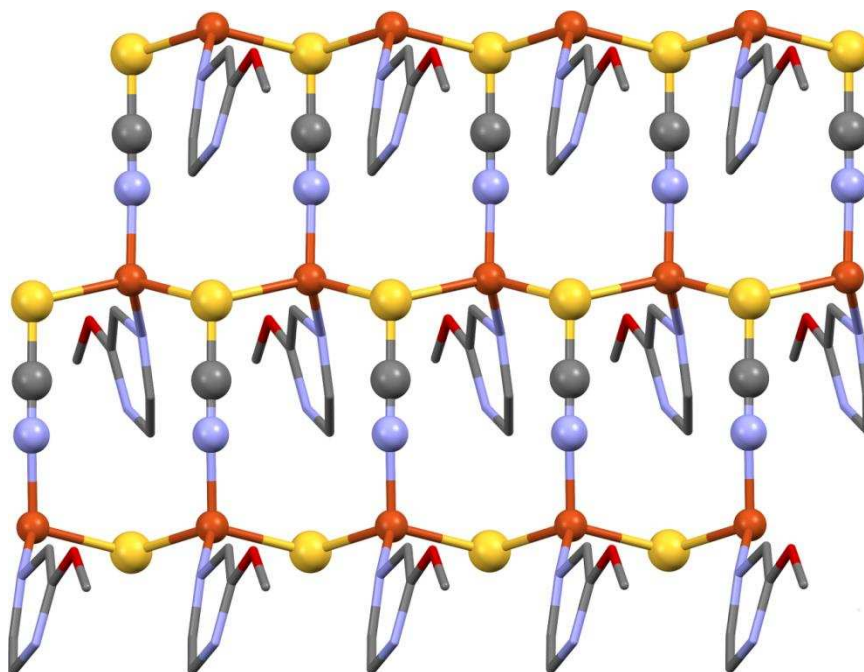


Figure 27. Networking diagram of **9**, viewed down the *b*-axis. Hydrogen atoms and disorder of the 2-MeOPyz have been omitted.

4.2.3 Structures of CuSCN-3-halopyridines

Compound **15a** crystallized as yellow prisms in the noncentrosymmetric monoclinic space group *Pc*. Crystals of **15a** were pseudomorphologically twinned, resulting in a major and a minor domain. Initial analysis of systematic absences in the twinned data suggested an orthorhombic *C* unit cell. The data were integrated and refined as a two-component twin with twin law $1\ 0\ 0 / 0\ -1\ 0 / -1\ 0\ -1$. As dictated by the 1:2 stoichiometry and the monodentate 3-ClPy ligand, the structure consists of 1-D chains of CuSCN of network Type A. Networking diagrams of **15a** are shown in Figure 28.

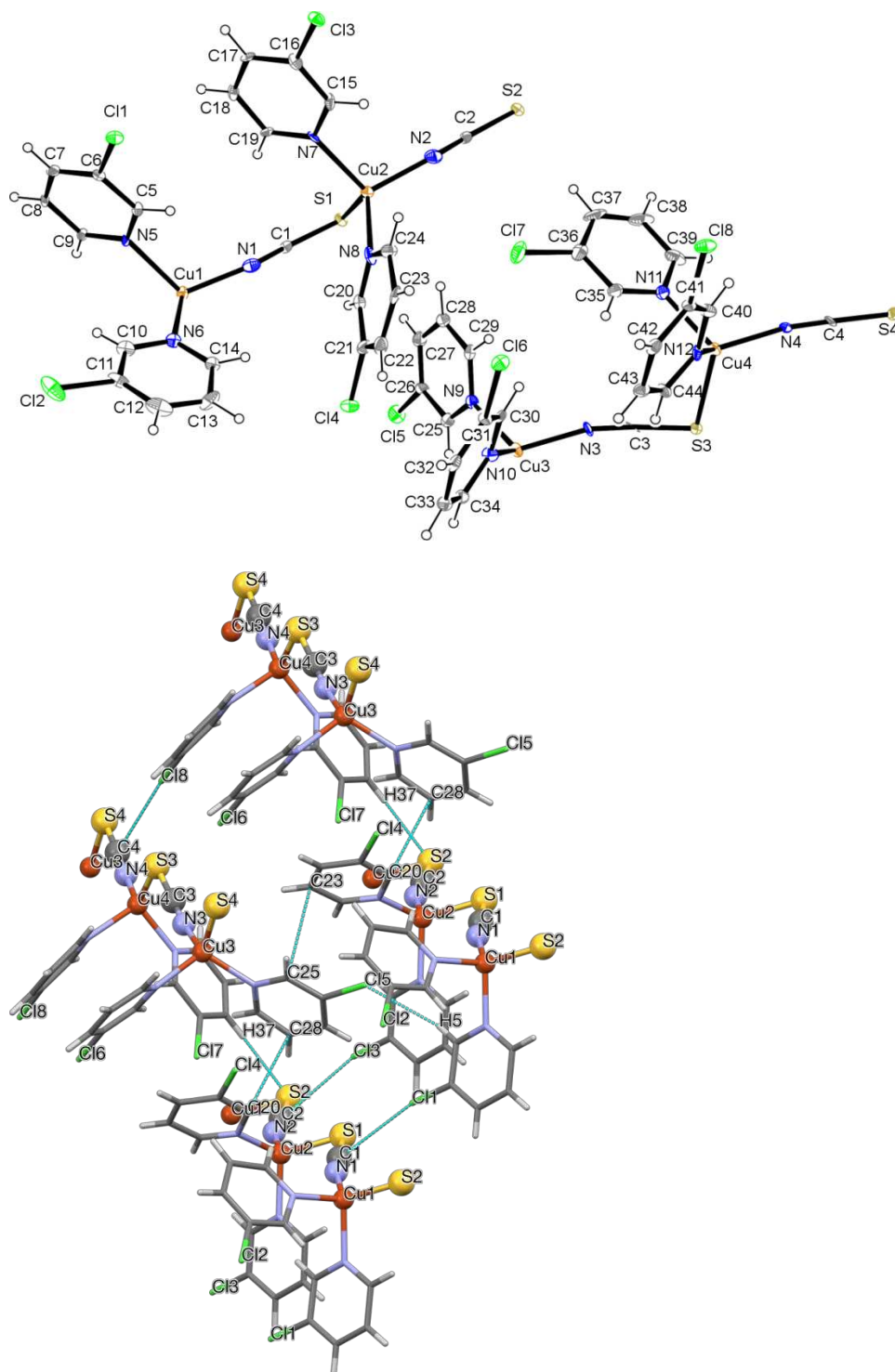


Figure 28. Structural diagrams of **15a**. Top: thermal ellipsoid rendering of the asymmetric unit. Bottom: diagram highlighting close interactions in the structure of **15a**

Unlike the other Type A networks described (**1a** and **4**), two independent chains are present in the unit cell. The first chain contains Cu1 and Cu2, while the second contains Cu3 and Cu4. The zig-zag angles of the first chain are Cu1–S2–C2 = 100.4(3) ° and N2–Cu2–S1 = 110.0(3) °. The corresponding angles for the second chain are Cu3–S4–C4 = 98.2(3) and N4–Cu4–S3 = 113.9(2)°. Bound to each copper atom are two 3-CIPy ligands. Within one chain, one pair of 3-CIPy ligands is canted in identical directions, while the other pair is canted in nearly orthogonal directions relative to one another. The angle formed by the planes of the 3-CIPy ligands containing Cl2 and Cl4 is 86.52°. Likewise, the interplanar angle of the 3-CIPy ligands containing Cl5 and Cl7 is 86.03°. This can be seen in the diagrams of Figure 29 showing the planes containing each 3-CIPy molecule. There are no π -stacking interactions between any of the 3-CIPy ligands.

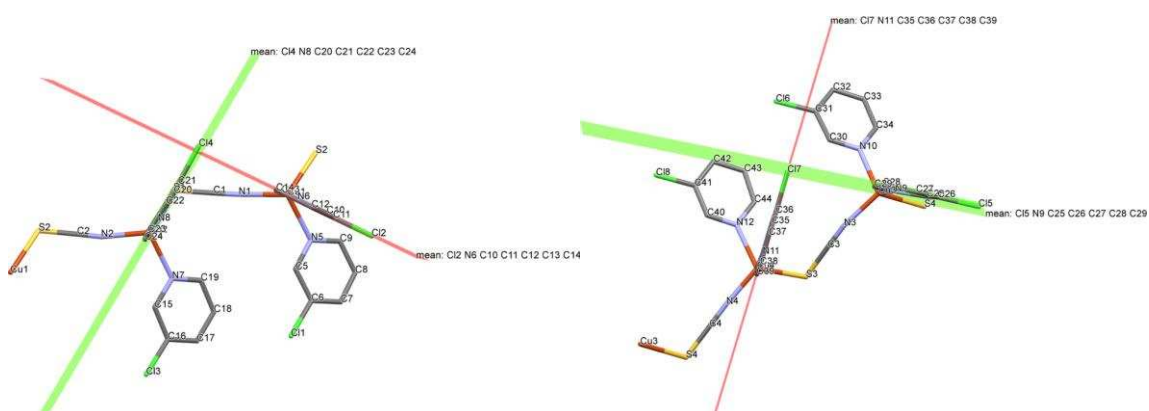


Figure 29. Diagrams showing angle between orthogonally canted 3-CIPy ligands. Left, chain 1; right, chain 2.

There are several potentially noteworthy interactions between the chlorine atoms of the Py rings and the carbons of the thiocyanate chains. The following bond distances fall within the van der Waals radii sums of Cl and C (3.45 Å): Cl1–C1 = 3.329(8) Å; Cl3–C2 = 3.375(8) Å; Cl8–C4 = 3.294(8) Å. A fourth potential interaction, Cl6–C3 = 3.466(9) Å, falls just outside the van der Waals radii sum. Each of these Cl–C interactions corresponds with a 3-CIPy ligand pair that is canted in the same direction. The

interactions are shown above in Figure 28. Additional close interactions are summarized in Table 3.

Atom 1	Atom 2	Distance (Å)
Cl1	C1 (SCN)	3.329(8)
Cl3	C2 (SCN)	3.375(8)
Cl6	C3 (SCN)	3.466(9)
Cl8	C4 (SCN)	3.294(8)
C20 (ClPy)	C28 (ClPy)	3.22(1)
C23 (ClPy)	C29 (ClPy)	3.30(1)
Cl4	H40 (ClPy)	2.882
S2	H37 (ClPy)	2.713
S3	H12 (ClPy)	2.737

Table 3. Close interactions between atoms in **15a**.

Compound **16a** also crystallized as yellow prisms in the non-centrosymmetric monoclinic space group *Pc*. The cell parameters of **16a** showed it to be isomorphic to **15a**. Like **15a**, crystals of **16a** were pseudomerohedrally twinned, first presenting with orthorhombic *C* symmetry. In addition, data collected from a preliminary crystal indicated the presence of a co-crystal of different symmetry. Data from a second crystal were used in solving the structure, and were integrated and refined as a two-component twin with twin law 1 0 0 / 0 -1 0 / -1 0 -1. The structure consists of two 1-D CuSCN chains decorated by 3-BrPy ligands. The zigzag angles of the first chain are Cu1–S2–C2 = 99.1(3)° and N2–Cu2–S1 = 114.7(3)°. The corresponding angles for the second chain are Cu3–S4–C4 = 98.1(3) and N4–Cu4–S3 = 115.3(2)°. Angles around copper centers range from 96.4(3)° to 115.3(2)°. The smaller angles around Cu correspond to the N_{amine}–Cu–N_{amine} angle. The CuSCN chains and 3-BrPy ligands are inverted within

the unit cell relative to the molecules of **15a**; this is apparent when viewed down the crystallographic *a*-axis. Figure 30 shows the contrast in orientation between the two structures.

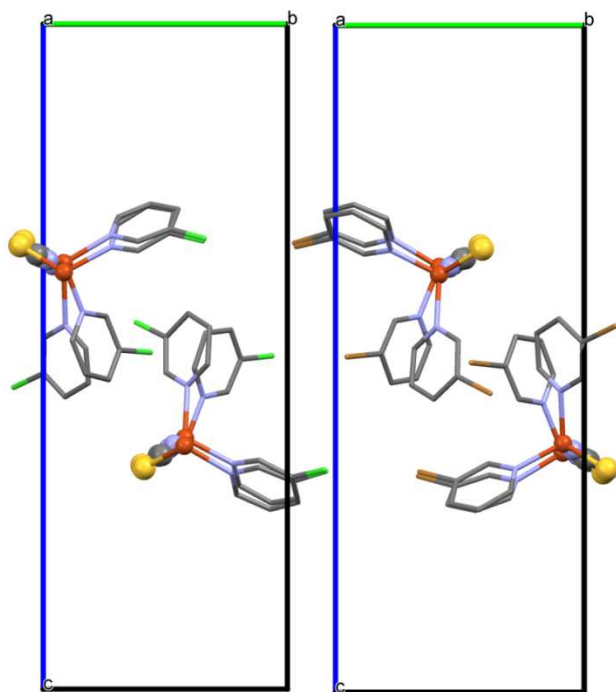


Figure 30. Side-by-side comparison of **15a** (left) and **16** (right) viewed along the *a*-axis.

Aside from orientation of the unit cell contents, the arrangement of chains and ligand molecules in both structures is comparable. Each independent CuSCN chain in **16a** has a pair of 3-BrPy ligands canted in the like direction and a pair of ligands oriented in nearly orthogonal directions relative to one another. The interplanar angles between the ligand molecules containing Br2 and Br4 is 87.30°; the corresponding angle between Br6 and Br8 is 87.14°.

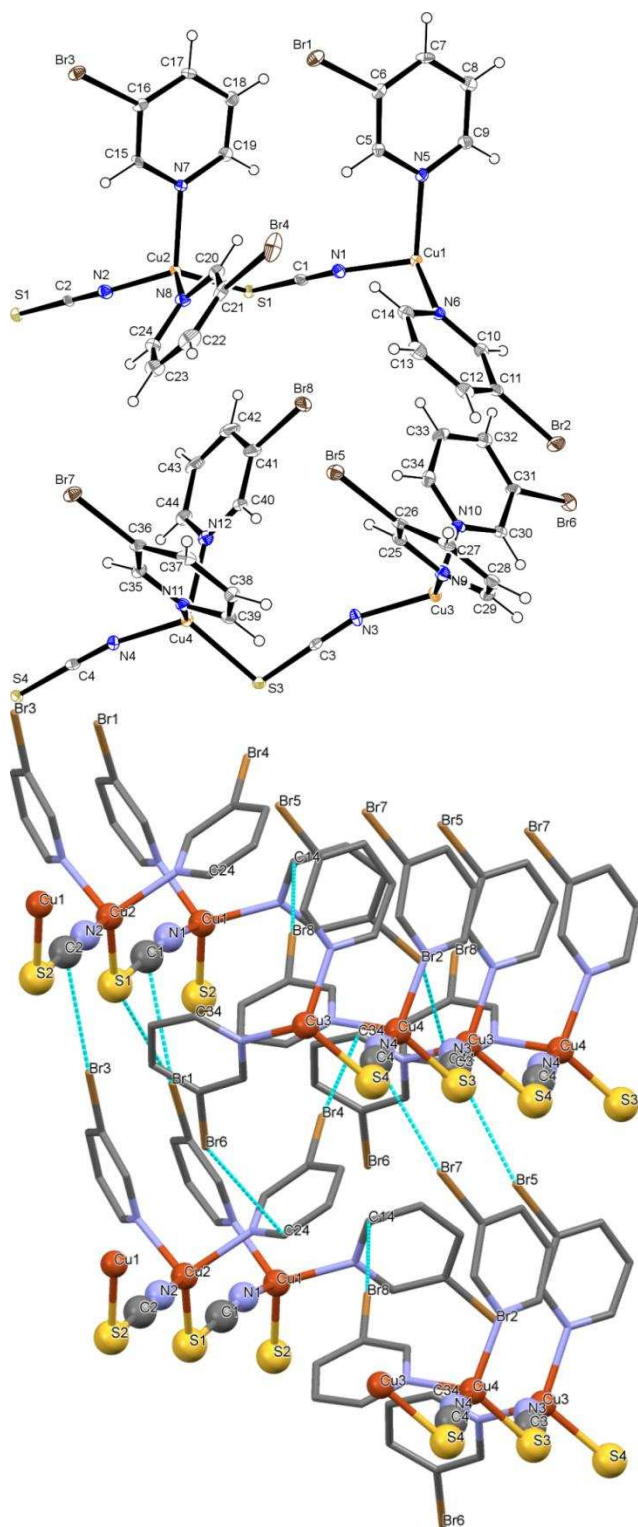


Figure 31. Structural diagrams of **16a**. Top: Thermal ellipsoid rendering of the asymmetric unit. Bottom: diagram highlighting C \cdots Br and S \cdots Br interactions between chains. Hydrogen atoms have been omitted.

As seen in the bottom diagram of Figure 31, the network contains numerous close interactions between the bromine atoms on the pyridine rings and either the sulfur atoms of the CuSCN chain or carbon atoms of nearby aromatic rings. Table 4 below summarizes the close interactions. Of special note are those of Br1, which interacts with both the sulfur (S1) and carbon (C1) atoms of the neighboring chain. As was the case with **15a**, the canting of the 3-BrPy rings seems to be indicative of favorable interactions between adjacent CuSCN chains and the ligand molecules. Pyridine rings containing Br1, Br3, Br5 and Br7 are oriented such that the bromine substituents point towards the thiocyanate chain. Ligand molecules containing Br2, Br4, Br6 and Br8 are oriented such that bromine atoms point directly to the arene of a neighboring pyridine.

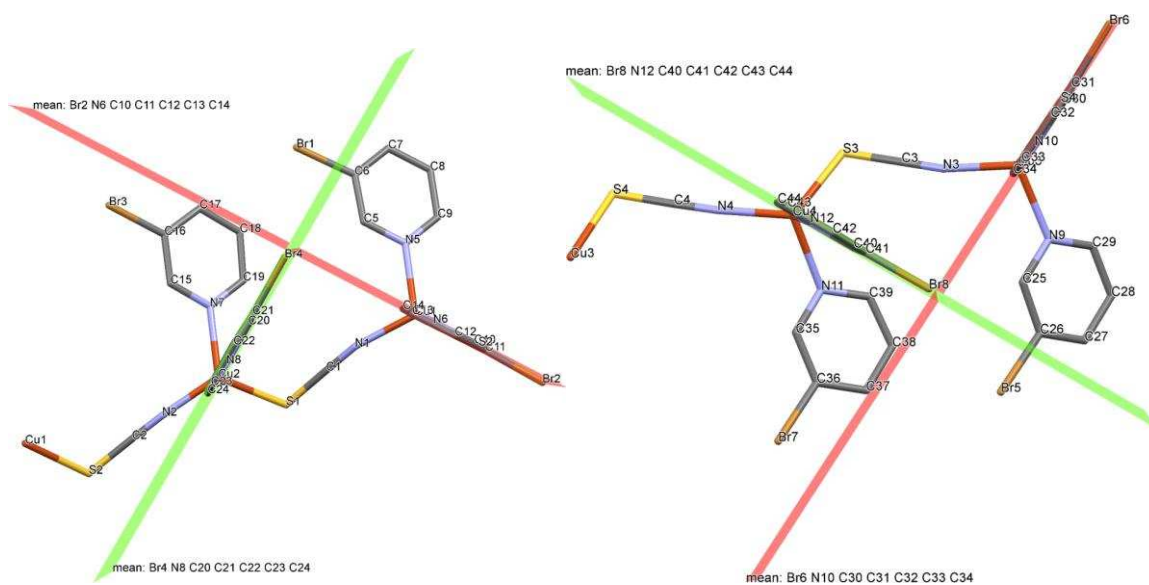


Figure 32 Diagrams showing angle between planes containing orthogonally canted pyridine ligands. Top, chain containing Br1-Br4; bottom, chain containing Br5-8.

Atom 1	Atom 2	Distance (Å)
Br1	C1 (SCN)	3.42(1)
Br1	S1 (NCS)	3.614(2)
Br2	C44 (BrPy)	3.49(1)
Br3	C2 (SCN)	3.369(9)
Br4	C34 (BrPy)	3.46(1)
Br5	C3 (SCN)	3.46(1)
Br6	C24 (BrPy)	3.47(1)
Br7	C4 (SCN)	3.34(1)
Br8	C14 (BrPy)	3.47(1)

Table 4: Potential bonding interactions in **16a**.

Lastly, compound **15c** crystallized as dark green plates in the centrosymmetric space group *C2/c*. Due to the combination of a copper(II) center and monodentate 3-ClPy ligand, the structure is a simple monomer of $\text{Cu}(\text{SCN})_2(3\text{-ClPy})_4$. The coordination environment about the copper center is nearly perfectly octahedral, with bond angles ranging from 89.15° to 90.85° . Bond lengths for ligands along the same axis are identical; $\text{Cu}-\text{N1}(\text{CS}) = 1.964 \text{ \AA}$, $\text{Cu}-\text{N2} = 2.064 \text{ \AA}$; $\text{Cu}-\text{N3} = 2.496 \text{ \AA}$. The relatively long $\text{Cu}-\text{N3}$ is indicative of Jahn-Teller distortion. Though there are no covalent connections between neighboring units, a relatively close distance between S1 and Cl2 of $3.2817(8) \text{ \AA}$ indicates a close interaction that may contribute to the close packing of the monomer units in the unit cell.

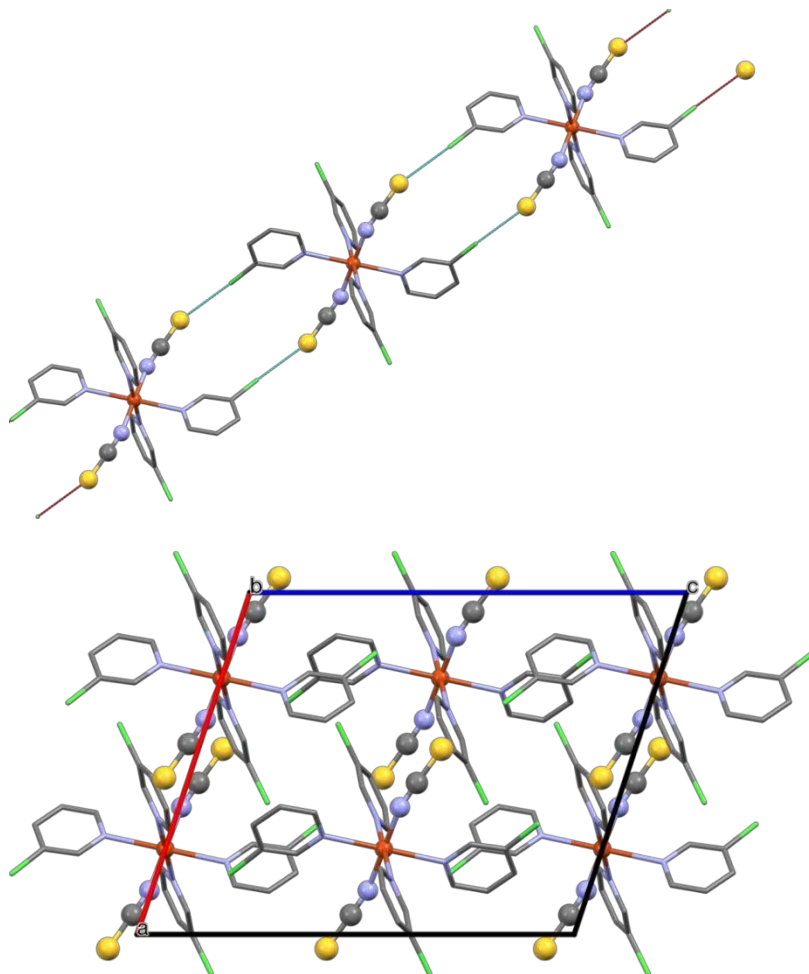


Figure 33. Diagram of **15c**. Top: view along the *b*-axis with Cl-S interactions shown. Bottom: packing diagram viewed along the *b* axis.

4.3 Optical Memory Results

4.3.1 Aromatic Amine Networks

A total of six CuSCN-aromatic amine networks were subjected to optical memory experiments, including three networks containing diimines (**10**, **11**, and **12**) and three compounds containing 3-XPy ligands (**15a**, **16**, **17**). Three of these compounds displayed evidence of optical memory. Compound **10**, initially the network of interest based on preliminary experiments, failed to produce evidence of optical memory.

(CuSCN)₂(2,3-Me₂Pyz) (**11**). Samples of **11** demonstrated a moderate reduction in emission intensity after irradiation by 266 nm laser light. The initial 5 min. period of

irradiation resulted in a 16% loss of emission intensity, followed by smaller losses after each successive irradiation interval. Attempted recovery of the emission by thermal cycling led only to a partial recovery of 84% of the original emission intensity. Due to this, only one cycle was run for **11**. The poor recovery capabilities of **11** preclude its use as a durable, rewriteable optical memory material.

Cycle 1- Compound 11			
Stage of cycle	Emission Intensity (a.u)	Change from initial (a.u)	Percent of total
Unexposed	1.2022×10^8	--	100
5 min exposure	1.0163×10^8	-1.86×10^7	84
10 min exposure	9.4970×10^7	-2.53×10^7	79
15 min exposure	9.1276×10^7	-2.89×10^7	76
20 min exposure	8.6934×10^7	-3.33×10^7	72
Post-recovery	1.0052×10^8	-1.97×10^7	84

Table 5. Peak emission intensities of **11**, before and after laser exposure and thermal cycling.

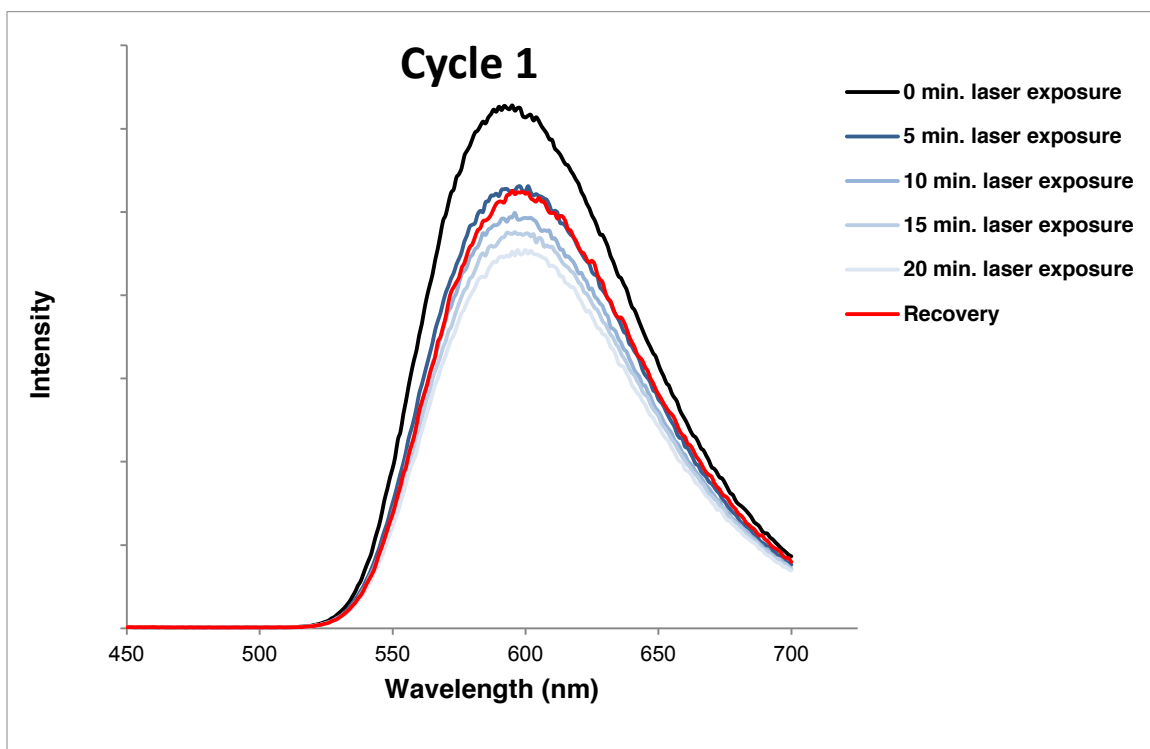


Figure 34: Emission for **11** excited at 373nm, taken at 80K.

(CuSCN)₂(2,5-Me₂Pyz) (**12**): Samples of **12** showed significant reduction in

emission intensity (75%) after the first 5 min interval of laser irradiation. Further irradiation reduced the intensity to a minimum of 13% after a total of 20 minutes. The first thermal cycling led to a recovery of to 94% of the original emission intensity. The samples were subjected to two more write/read/erase cycles. The second and third cycles showed decay in the emission maximum after recovery, first to 73% of the recovered intensity, then to 67% after cycle 3. The decay issue becomes more apparent when comparing the post-recovery intensities to that of the unexposed sample; recovery after cycle 2 is only 68% of the initial intensity, while recovery after cycle 3 is only 46% the initial emission intensity. Therefore, while **12** undergoes a rapid loss in emission favorable for writing, the lack of resiliency after multiple cycles limits its promise for optical memory.

Cycle 1- Compound 12			
Stage of cycle	Emission Intensity (a.u)	Change from initial (a.u)	Percent of total
Unexposed	1.68×10^8	--	100
5 min exposure	4.17×10^7	-1.26×10^8	25
10 min exposure	3.18×10^7	-1.36×10^8	19
15 min exposure	2.60×10^7	-1.42×10^8	15
20 min exposure	2.22×10^7	-1.46×10^8	13
Post-recovery	1.58×10^8	-1.05×10^7	94

Cycle 2- Compound 12			
Stage of cycle	Emission Intensity (a.u)	Change from initial (a.u)	Percent of total
Unexposed	1.58×10^8	--	100
5 min exposure	3.63×10^7	-1.21×10^8	23
10 min exposure	2.74×10^7	-1.30×10^8	17
15 min exposure	2.17×10^7	-1.36×10^8	14
20 min exposure	1.88×10^7	-1.39×10^8	12
Post-recovery	1.15×10^8	-4.24×10^7	73

Cycle 3- Compound 12			
Stage of cycle	Emission Intensity (a.u)	Change from initial (a.u)	Percent of total
Unexposed	1.15×10^8	--	100
5 min exposure	3.65×10^7	-7.87×10^7	32
10 min exposure	2.60×10^7	-8.92×10^7	23
15 min exposure	2.18×10^7	-9.34×10^7	19
20 min exposure	1.89×10^7	-9.62×10^7	16
Post-recovery	7.71×10^7	-3.81×10^7	67

Table 6. Emission intensities of **12**, before and after laser exposure and thermal cycling.

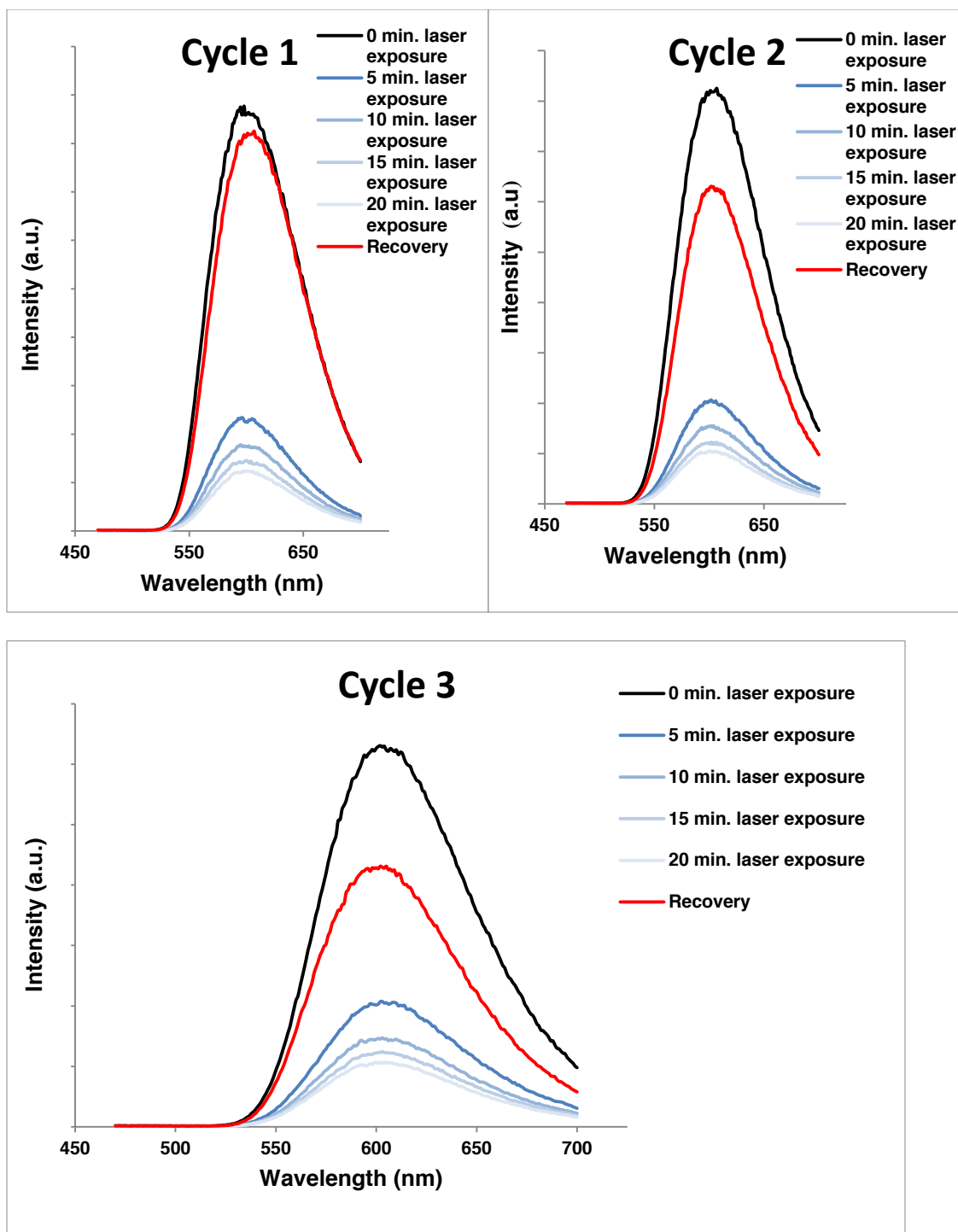


Figure 35: Emission spectra for **12** excited at 375nm at 80 K after the first (top left), second (top right), and third (bottom) write/read/erase cycles.

(CuSCN)(3-ClPy)₂ (**15a**). Samples of **15a** showed no notable reduction in emission intensity after irradiation with four different wavelengths (318, 270, 239, and

210 nm) for 5 min intervals, up to 20 minutes of total laser exposure. The broad, intense peak centered at 491 nm does not shift after the maximum 20-min laser exposure time, and its intensity is not significantly altered. Time-dependent density functional theory (TD-DFT) calculations of the excited states associated with these laser wavelengths likewise yielded no reduction in predicted intensity of emissions. The most probable excited state, associated with the 240 nm laser wavelength, results in the elongation of a Cu–S bond (2.41 Å to 2.72 Å) and contracting of S–C and Cu–N bonds (1.74 Å to 1.69 Å and 2.04 Å to 1.93 Å, respectively). No change in the C–Cl bonds is observed in any excited states associated with the four laser wavelengths.

(CuSCN)(3-BrPy)₂ (**16a**). Compound **16** demonstrated the most remarkable luminescence behavior of any compound during the course of the optical memory experiments. The emission shows an intense and broad peak centered at 540 nm that remains unshifted during the course of the experiments. During the first cycle, a 77% reduction in emission intensity was achieved after the first 5-minute irradiation period. A maximum reduction of 88% was achieved after the full 20 min. of irradiation. A thermal cycle resulted in complete recovery of the emission peak intensity, given as 112%. It should be noted that this is not indicative of an increase in emission intensity, but is merely the post-recovery signal strength relative to the initial intensity. Two additional cycles were performed on the sample, each time resulting in complete recovery of the pre-exposure emission levels. A noticeable difference between cycles can be seen in the change of emission intensity after the first 5-minute interval; cycle 2 achieves only a 57% reduction in signal strength, while cycle 3 achieves only a 33% reduction after the first 5 minute exposure. The percent reduction after 15 and 20 minutes intervals remains consistent across the three cycles however.

Cycle 1- Compound 16a			
Stage of cycle	Emission Intensity (a.u)	Change (a.u)	Percent of initial
Unexposed	2.87×10^8	--	100
5 min exposure	6.64×10^7	-7.87×10^7	23
10 min exposure	6.79×10^7	-8.92×10^7	24
15 min exposure	4.94×10^7	-9.34×10^7	17
20 min exposure	3.51×10^7	-9.62×10^7	12
Post-recovery	3.21×10^8	3.35×10^7	112*

Cycle 2- Compound 16a			
Stage of cycle	Emission Intensity (a.u)	Change (a.u)	Percent of initial
Unexposed	3.21×10^8	--	100
5 min exposure	1.38×10^8	-1.83×10^8	43
10 min exposure	1.87×10^8	-1.34×10^8	58
15 min exposure	6.99×10^7	-2.51×10^8	22
20 min exposure	4.09×10^7	-2.80×10^8	13
Post-recovery	3.11×10^8	-9.46×10^7	97

Cycle 3- Compound 16a			
Stage of cycle	Emission Intensity (a.u)	Change (a.u)	Percent of initial
Unexposed	3.11×10^8	--	100
5 min exposure	2.09×10^8	-1.03×10^8	67
10 min exposure	6.45×10^7	-2.47×10^8	21
15 min exposure	4.11×10^7	-2.70×10^8	13
20 min exposure	3.92×10^7	-2.72×10^8	13
Post-recovery	3.18×10^8	7.04×10^6	102*

Table 7. Emission intensity changes before and after laser irradiation intervals and thermal cycles.

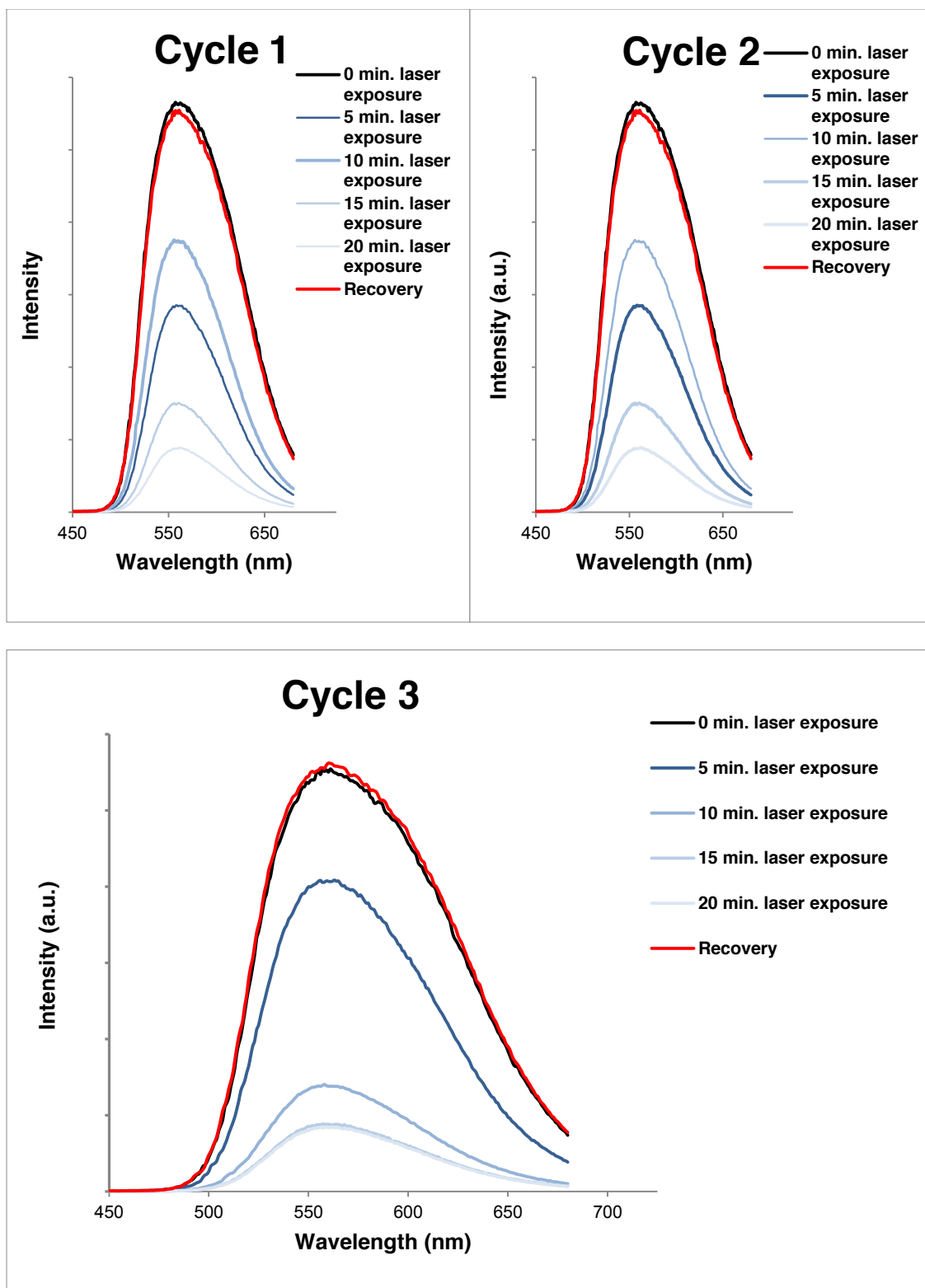


Figure 36: Emission spectra for **16** excited at 376nm at 80 K after the first (top left), second (top right), and third (bottom) write/read/erase cycles.

TD-DFT calculations indicate that the 266-nm irradiation wavelength likely results in an increased C–Br bond length, from 1.96 Å to 2.27 Å. This excited state corresponds with a reduced emission spectrum. The elongated bond was the only structural difference between excited states that continue to emit and the nonemissive excited state. As was noted in the discussion of the crystal structure, several bromine atoms on the pyridine ligands have close interactions with neighboring carbocyclic rings and SCN chains. It is plausible that elongation of the C–Br bond disrupts these intermolecular interactions, leading to the loss of emission after exposure to high-energy radiation.

(CuSCN)(3-IPy) (**17**). Compound **17** did not produce sufficient changes in emission after exposure to high-energy laser radiation. A maximum reduction in intensity of 6% was achieved after the total exposure time of 20 minutes, and the system recovered to nearly 100% after a thermal recovery cycle. However, the modest emission reduction, coupled with the amount of time necessary to achieve a notable change, precluded the continued use of **17** in further experiments.

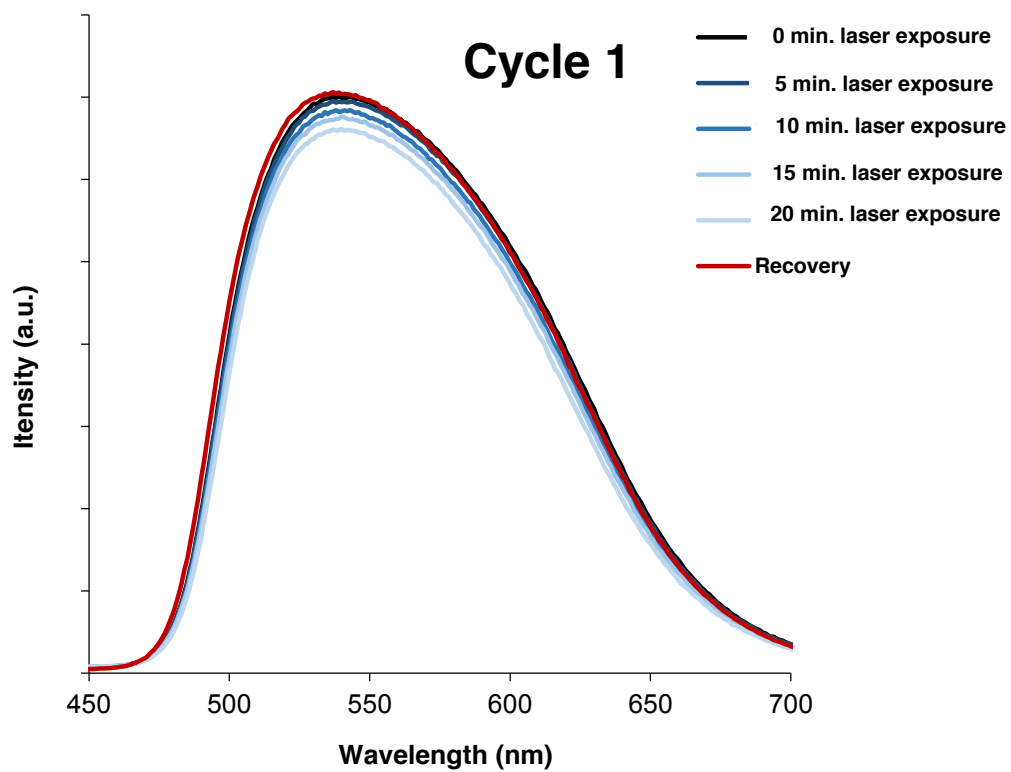


Figure 37: Emission spectra for **17** excited at 398nm at 80 K.

Conclusion

A total of twenty compounds were synthesized, characterized and studied using UV/Vis emission spectroscopy during the course of the work presented in this thesis. A combination of synthetic techniques was used to obtain the compounds. An aqueous reflux of a suspension containing CuSCN, ligand, ammonia and KSCN yielded pure products of seven CuSCN-diimine compounds. Bulk samples were obtained by stirring the mixture, while single crystals were obtained by allowing the mixture to reflux without stirring. Compounds for which this technique proved unsuccessful could be obtained by directly reacting CuSCN with the neat ligand, either in sealed vessels at room temperature or as solids in an oven. Twelve novel crystal structures were solved, including four CuSCN-alkyl sulfide networks of a previously unreported class of compounds, five luminescent CuSCN-diimine networks that may warrant further optical memory experiments, and three CuSCN-3-XPY networks, whose structures had not previously been known. In the case of **15c**, the compound itself had not yet been reported.

Optical memory experiments run on a series of CuSCN-aromatic amine networks yielded mixed results. Some compounds, including **10** and **15a**, failed to demonstrate any potential optical memory at the selected wavelengths. Others, including **11** and **12**, suffered from severe fatigue after a single irradiation/recovery cycle. Compound **16a** produced promising memory behavior, including complete recovery, even after three irradiation/recovery cycles. Computational modeling indicates changes in the bromine-carbon bond distance, which may impact intermolecular interactions within the packed chain network of **16a**. These broken interactions may play a role in the loss of emission upon exposure to high-energy radiation.

APPENDIX

Table A1. Crystal and Structure Refinement Data.

complex	1a	2	3	4
CCDC deposit no.	1460762	1460764	1460765	1460763
color and habit	colorless block	colorless prism	colorless prism	colorless plate
size, mm	0.49 × 0.42 × 0.26	0.45 × 0.14 × 0.11	0.63 × 0.10 × 0.08	0.38 × 0.21 × 0.06
formula	C ₅ H ₁₂ CuNS ₃	C ₅ H ₁₀ CuNS ₂	C ₇ H ₁₄ CuNS ₂	C ₉ H ₁₆ CuNS ₃
formula weight	245.88	211.80	239.85	297.95
space group	<i>P</i> 2 ₁ / <i>c</i>	<i>P</i> 2 ₁ / <i>n</i>	<i>P</i> 2 ₁ / <i>n</i>	<i>P</i> 2 ₁
<i>a</i> , Å	7.39230(10)	5.82340(10)	5.92320(10)	5.8965(2)
<i>b</i> , Å	13.0297(3)	9.6077(2)	10.9226(2)	9.3775(3)
<i>c</i> , Å	11.2206(2)	16.2675(4)	15.9989(3)	11.7823(3)
β, deg	108.7360(10)	96.4230(10)	91.4730(10)	98.004(2)
volume, Å ³	1023.49(3)	904.45(3)	1034.73(3)	645.15(3)
<i>Z</i>	4	4	4	2
ρ _{calc} , g cm ⁻³	1.596	1.555	1.540	1.534
<i>F</i> ₀₀₀	504	432	496	308
μ(Cu Ka), mm ⁻¹	8.211	7.093	6.271	6.626
temperature, K	100(2)	296(2)	100(2)	296(2)
residuals: ^a <i>R</i> ; <i>R</i> _w	0.0232; 0.0581	0.0327; 0.0936	0.0228; 0.0589	0.0294; 0.0737
goodness of fit	1.209	1.038	0.997	1.103
Flack	—	—	—	0.03(4)

Table A1 cont.

complex	5	6	7
CCDC deposit no.	1460758	1460757	1460759
color and habit	orange prism	yellow plate	yellow block
size, mm	$0.39 \times 0.10 \times 0.07$	$0.18 \times 0.12 \times 0.05$	$0.22 \times 0.17 \times 0.12$
formula	$\text{C}_{10}\text{H}_6\text{Cu}_2\text{N}_4\text{S}_2$	$\text{C}_9\text{H}_6\text{CuN}_3\text{S}$	$\text{C}_{10}\text{H}_6\text{Cu}_2\text{N}_4\text{S}_2$
formula weight	373.39	251.77	373.39
space group	$P2_1/n$	Cc	$Pbca$
a , Å	5.86660(10)	21.6629(4)	13.3325(3)
b , Å	17.5548(4)	3.76380(10)	10.8446(2)
c , Å	11.7576(3)	11.2315(2)	16.6635(3)
α , deg	90	90	90
β , deg	97.8520(10)	101.4430(10)	90
γ , deg	90	90	90
volume, Å ³	1199.53(5)	2118.51(6)	3837.12(16)
Z	4	4	8
ρ_{calc} , g cm ⁻³	2.068	1.863	2.059
F_{000}	736	504	1472
$\mu(\text{Cu K}\alpha)$, mm ⁻¹	2.068	1.863	2.059
temperature, K	100(2)	100(2)	100(2)
residuals: ^a R ; R_w	0.0330; 0.0843	0.0432; 0.1328	0.0201; 0.0577
goodness of fit	1.049	1.091	1.055
Flack	–	0.03(4)	–

Table A1. Cont'd.

complex	8	9
CCDC deposit no.	1460761	1460760
color and habit	yellow block	colorless blade
size, mm	$0.13 \times 0.11 \times 0.06$	$0.36 \times 0.09 \times 0.04$
formula	$\text{C}_6\text{H}_5\text{Cu}_2\text{N}_5\text{S}_2$	$\text{C}_6\text{H}_6\text{CuN}_3\text{OS}$
formula weight	338.35	231.74
space group	<i>P</i> −1	<i>Pnnm</i>
<i>a</i> , Å	5.7586(2)	10.4822(2)
<i>b</i> , Å	6.6582(2)	20.7412(4)
<i>c</i> , Å	7.1610(3)	3.81760(10)
α , deg	103.521(2)	90
β , deg	97.653(2)	90
γ , deg	111.017(2)	90
volume, Å ³	241.968(15)	830.00(3)
<i>Z</i>	1	4
ρ_{calc} , g cm ^{−3}	2.068	1.855
<i>F</i> ₀₀₀	166	464
$\mu(\text{Cu K}\alpha)$, mm ^{−1}	9.211	5.690
temperature, K	100(2)	100(2)
residuals: ^a <i>R</i> ; <i>R</i> _w	0.0281; 0.0675	0.0276; 0.0707
goodness of fit	1.078	1.055
Flack	–	–

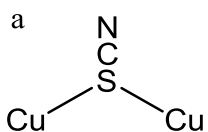
Table A1 cont.

	15a	15c	16
CCDC deposit no.	(Not yet sent)	(Not yet sent)	(Not yet sent)
color and habit	yellow prism	green prism	yellow block
size, mm	0.52 × 0.15 × 0.14	0.498 × 0.173 × 0.064	0.28 × 0.23 × 0.10
formula	C ₄₄ H ₃₂ Cl ₈ Cu ₄ N ₁₂ S ₄	C7.33 H5.33 Cl1.33 Cu0.33 N2 S0.67	C ₄₄ H ₃₂ Br ₈ Cu ₄ N ₁₂ S ₄
formula weight	1394.81	211.29	1750.49
space group	<i>Pc</i>	<i>C2/c</i>	<i>Pc</i>
<i>a</i> , Å	11.4848(2)	13.7524(2)	11.5742(2)
<i>b</i> , Å	9.2543(2)	12.0934(2)	9.4358(2)
<i>c</i> , Å	25.8293(5)	16.7134(2)	25.9158(5)
β, deg	102.8390(7)	108.2580(10)	102.9110(10)
volume, Å ³	2676.59(9)	2639.72(7)	2758.76(9)
<i>Z</i>	2	12	2
ρ _{calc} , g cm ⁻³	1.731	1.595	2.107
<i>F</i> ₀₀₀	1392	1276	1680
μ(Cu Ka), mm ⁻¹	7.303		10.310
temperature, K	100(2)	100(2)	100(2)
residuals: ^a <i>R</i> ; <i>R</i> _w	0.0395; 0.0987	0.0213, 0.0544	0.0303; 0.0797
goodness of fit	1.032	1.041	1.044
Flack	0.040(8)	-	0.200

^a*R* = *R*₁ = Σ||*F*_o| - |*F*_c|| / Σ|*F*_o| for observed data only. *R*_w = *wR*₂ = {Σ[*w*(*F*_o² - *F*_c²)²] / Σ[*w*(*F*_o²)²]}^{1/2} for all data.

Table A2. Selected Bond Distances (Å) and Angles (deg).

	1	2	3	4
Cu–SCN	2.3784(5)	2.3684(11), 2.5004(10)	2.3883(5), 2.4816(5)	2.3438(15)
S–C	1.6550(19)	1.658(3)	1.6677(19)	1.648(5)
C–N	1.158(3)	1.142(4)	1.158(3)	1.143(6)
Cu–NCS	1.9493(17)	1.961(3)	1.9629(16)	1.967(5)
Cu–SR ₂	2.2868(5), 2.3456(5)	2.227(6)	2.2739(5)	2.187(19), 2.400(17)
Cu···Cu	–	2.8895(10)	3.1662(6)	–
Cu–S–C	96.41(7)	95.30(11), 106.60(12)	97.08(7), 107.43(7)	105.07(18)
S–C–N	179.19(18)	178.5(3)	177.41(18)	178.3(5)
C–N–Cu	170.51(16)	161.2(2)	160.64(15)	173.4(4)
Cu–S–Cu ^a	–	72.75(3)	81.084(17)	–
SCN–Cu–SCN	106.73(5)	104.35(10), 103.16(8)	103.06(5), 107.81(5)	110.06(15)
NCS–Cu–SCN	–	107.25(3)	98.917(17)	–
SCN–Cu–SR ₂	106.78(5), 117.24(5)	114.62(19)	115.60(5)	103.5(3), 109.6(6)
NCS–Cu–SR ₂	104.328(19), 108.974(19)	103.97(14), 121.80(12)	107.924(19), 120.75(2)	109.8(4), 117.7(6)
R ₂ S–Cu–SR ₂	111.904(19)	–	–	105.0(6)



	5	6	7
Cu–SCN	2.3185(9), 2.2788(9), 2.4641(9), 2.5641(9)	2.345(2), 2.349(2)	2.3641(5), 2.3883(5), 2.3994(5), 2.4814(5)
S–C	1.667(3), 1.668(3)	1.672(10)	1.664(2), 1.666(2)
C–N	1.156(4), 1.159(4)	1.150(13)	1.156(3), 1.161(3)
Cu–NCS	1.975(3), 1.983(3)	1.953(8)	1.9035(18), 1.9272(17)
Cu–N _{arom}	2.019(3), 2.032(3)	2.057(7)	2.0038(16), 2.0839(16)
Cu···Cu	2.7305(6)	–	3.0417(4)
Cu–S–C	93.99(11), 106.04(11)	104.8(3), 108.3(3)	100.11(7), 100.69(6), 100.70(7), 102.25(7)
S–C–N	177.3(3), 177.9(3)	177.9(8)	178.52(18), 179.54(19)
C–N–Cu	161.7(3), 162.9(3)	177.5(7)	173.56(16), 177.13(16)
Cu–S–Cu ^a	67.79(3), 70.17(3)	106.60(8)	77.083(16), 109.84(2)
SCN–Cu–SCN	101.53(8), 103.02(8), 107.27(8), 108.80(8)	106.30(19), 111.6(2)	102.74(5), 105.19(5), 109.62(5), 112.70(5)
NCS–Cu–SCN	109.92(3), 112.12(3)	106.60(8)	108.996(19), 117.592(19)
SCN–Cu–N _{arom}	104.29(11), 108.59(11)	109.23(18), 112.4(3)	120.52(7), 134.53(7)
NCS–Cu–N _{arom}	100.56(8), 105.23(8), 119.39(8), 128.49(8)	110.52(18)	93.58(4), 97.13(5), 102.16(5), 106.66(5)

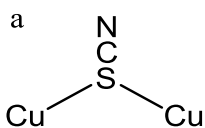
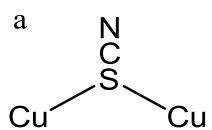


Table A2. Cont'd.

	8	9
Cu–SCN	2.3576(7), 2.6790(9)	2.3513(5)
S–C	1.659(3)	1.672(4)
C–N	1.159(4)	1.149(5)
Cu–NCS	1.975(3), 1.983(3)	1.944(3)
Cu–N _{arom}	1.996(2)	2.041(3)
Cu···Cu	3.0032(10)	–
Cu–S–C	96.70(9), 101.91(9)	102.69(6)
S–C–N	178.0(3)	177.8(3)
C–N–Cu	164.0(2)	170.0(2)
Cu–S–Cu ^a	72.89(2)	108.55(3)
SCN–Cu–SCN	97.59(7), 107.73(7)	105.71(5)
NCS–Cu–SCN	107.11(2)	108.55(3)
SCN–Cu–N _{arom}	134.75(10)	115.91(11)
NCS–Cu–N _{arom}	93.92(7), 110.27(7)	110.31(5)



	15a	16
	(CuSCN)(3-ClPy) ₂	(CuSCN)(3-BrPy) ₂
Cu–S	2.286(3), 2.328(3), 2.344(2), 2.305(2)	2.300(3), 2.331(3), 2.295(3), 2.342(3)
S–C	1.696(9), 1.699(9), 1.647(10), 1.641(9)	1.656(10), 1.673(10), 1.666(10), 1.659(10)
C–N	1.092(12), 1.105(12), 1.155(12), 1.168(11)	1.157(14), 1.145(13), 1.158(13), 1.158(13)
Cu–NCS	1.972(10), 1.974(9), 1.950(7), 1.921(7)	1.963(9), 1.935(9), 1.946(9), 1.942(9)
Cu–N _{Py}	2.034(7), 2.115(7), 2.068(8), 2.107(7), 2.062(7), 2.086(7), 2.050(7), 2.091(7)	2.069(8), 2.087(8), 2.076(8), 2.101(7), 2.073(8), 2.087(8), 2.060(8), 2.098(8)
Cu–S–C	98.8(3), 100.5(3), 99.4(3), 98.1(3)	100.1(3), 99.1(3), 101.2(3), 98.1(3)
S–C–N	177.4(9), 175.6(10), 175.4(8), 177.8(9)	178.5(9), 179.0(9), 179.0(9), 178.3(9)
C–N–Cu	166.7(9), 160.6(9), 165.9(8), 171.5(7)	164.3(8), 168.6(8), 163.2(8), 170.0(8)
SCN–Cu–SCN	113.6(2), 109.9(3), 109.5(3), 113.9(2)	111.6(3), 114.7(3), 111.5(3), 115.3(2)
SCN–Cu–N _{arom}	110.7(3), 113.3(3), 112.9(3), 107.0(3), 105.4(3), 113.8(3), 112.3(3), 110.0(3)	113.3(3), 105.6(3), 110.7(3), 112.7(3), 113.4(3), 106.2(3), 111.0(3), 110.9(3)
N _{arom} –Cu–N _{arom}	96.4(3), 111.1(3), 112.5(3), 97.6(3)	110.2(3), 96.5(3), 111.1(3), 97.1(3)

NCS–Cu–N _{arom}	115.8(2), 105.72(19),	106.5(2), 109.7(2),
	107.8(2), 108.1(2),	114.3(2), 106.5(2),
	109.1(2), 106.5(2),	106.0(2), 108.6(2),
	113.8(2), 107.7(2)	113.4(2), 107.7(2)

15c

Complex	Cu(SCN) ₂ (3-CIPy) ₄
S–C	1.6255(15)
C–NCS	1.166(2)
Cu–NCS	1.9642(12)
Cu–N _{Arom}	2.0637(12), 2.496
Cu–S–C	89.18(5)
S–C–N	178.77(14)
C–N–Cu	158.55(12)
N _{arom} –Cu–N _{arom}	89.18(5), 90.82(5)

REFERENCES

1. R. Q. Snurr, J. T. Hupp, S. T. Nguyen. *AIChE J.* **2004**, *50*, 1090.
2. M. Hirscher, B. Panella, *Scr. Mater.* **2007**, *56*, 809. (b) N. Sakai, S. Matile. *Angew. Chem., Int. Ed.* **2008**, *47*, 9603. (c) B. Schmitz, U. Müller, N. Trukhan, M. Schubert, G. Férey, M. I. Hirscher. *Chem. Phys. Chem.* **2008**, *9*, 2181.
3. K. Ding, L. Wang, L. Shi, *Pure Appl. Chem.* **2007**, *79*, 1531.
4. M. D. Dembo, L. E. Dunaway, J. S. Jones, E. A. Lepekhina, S. M. McCullough, J. L. Ming, X. Li, F. Baril-Robert, H. H. Patterson, C. A. Bayse, R. D. Pike. *Inorg. Chim. Acta* **2010**, *364*, 102.
5. K.K. Shin, J. D. Barrie, B. Dunn, I. J. I. Zink. *J. Am. Chem. Soc.* **1990**, *112*, 5701.
6. M. Kabesova, M. Dunaj-Jurco, M. Serator, J. Gazo. *Inorg. Chim. Acta* **1976**, *17*, 161.
7. D. L. Smith, V. I. Saunders. *Acta Crystallogr., Sect. B.* **1981**, *37*, 1807.
8. D. L. Smith, V. I. Saunders. *Acta Crystallogr., Sect. B* **1982**, *38*, 907.
9. P. C. Healy, C. Pakawatchai, R. I. Papasergio, V. A. Patrick, A. H. White. *Inorg. Chem.* **1984**, *23*, 3769.
10. K. M. Miller, S. M. McCullough, E. A. Lepekhina, I. J. Thibau, R. D. Pike. *Inorg. Chem.* **2011**, *50*, 7239.
11. M. A. S. Goher, F. A. Mautner. *Polyhedron* **1999**, *18*, 1805.
12. O. Teichert, W. S. Sheldrick. *Z. Anorg. Allg. Chem.* **1999**, *625*, 1860.
13. O. Teichert, W. S. Sheldrick, *Z. Anorg. Allg. Chem.* **2000**, *626*, 2196.
14. A.J. Blake, N.R. Champness, M. Crew, L.R. Hanton, S. Parsons, M. Schroder. *J. Chem. Soc., Dalton Trans.* **1998**, 1533.
15. A.J. Blake, N.R. Brooks, N.R. Champness, M. Crew, L.R. Hanton, P. Hubberstey, S. Parsons, M. Schroder. *J. Chem. Soc., Dalton Trans.* **1999**, 2813.
16. T. Otieno, J.R. Blanton, K.J. Lanham, S. Parkin, *J. Chem. Cryst.* **2003**, *33*, 335.

17. C.Näther, I.Jeß, P. Kowallik. *Z. Anorg. Allg. Chem.* **2003**, 629, 2144.
18. L. Li, R. Yuan, L. Liu, Z. Ren, A. Zheng, H. Cheng, H. Li, J. Lang. *Cryst. Growth Des.* **2010**, 10, 1929.
19. C.Näther, J. Greve, I.Jeß, C. Wickleder. *Solid State Sci.* **2003**, 5, 1167.
20. C. Näther, M.Wriedt, I.J Jeß. *Acta Crystallogr.,Sect.E:Struct.Rep.Online.* **2005**, 61, m329.
21. C. Näther, I. Jeß, *Acta Cryst.* **2004** C60, m153.
22. (a) H. O. House, C.-Y. Chu, J. M. Wilkins, J. J. Umen, *J. Org. Chem.* **1975**, 40, 1460.
 (b) B. H. Lipshutz, S. Whitney, J. A. Kozlowski, C. M. Breneman, *Tetrahedron Lett.* **1986**, 27, 4273. (c) S. H. Bertz, C. P. Gibson, G. Dabbagh, *Organometallics* **1988**, 7, 227.
23. (a) B. Lenders, D. M. Grove, W. J. J. Smeets, P. van der Sluis, A. L. Spek, G. van Koten. *Organometallics* **1991**, 10, 786. (b) H. Maelger, F. Olbrich, J. Kopf, D. Abein E. Weiss. *Z. Naturforsch.* **1992**, 47b, 1276. (c) J. Zhou, G.-Q. Bian, J. Dai, Y. Zhang, Q.-Y. Zhu, W. Lu. *Inorg. Chem.* **2006**, 45, 8486. (d) M. Heller W. S. Sheldrick. *Z. Anorg. Allg. Chem.* **2004**, 630, 1869. (e) K. M. Henline, C. Wang, R. D. Pike, J. C. Ahern, B. Sousa, H. H. Patterson, A. T. Kerr, C. L. Cahill. *Cryst. Growth Des.* **2014**, 14, 1449. (f) P. D. Harvey, M. Knorr. *J. Clust. Sci.* **2015**, 26, 411. (g) M. Knorr, A. Bonnot, A. Lapprand, A. Khatyr, C. Strohmann, M. M. Kubicki, Y. Rousselin, P. D. Harvey. *Inorg. Chem.* **2015**, 54, 4076. (h) A. Bonnot, M. Knorr, F. Guyon, M. M. Kubicki, Y. Rousselin, C. Strohmann, D. Fortin, P. D. Harvey. *Cryst. Growth Des.* **2016**, 16, 774. (i) T.Rottgers, W.S.Sheldrick. *Z. Anorg. Allg. Chem.* **2001**, 627, 1976.
24. (a) D. Li, T. Wu, X.-P. Zhou, R. Zhou, X.-C. Huang. *Angew. Chem., Int. Ed.* **2005**, 44, 4175. (b) J. Wang, Y.-H. Zhang, H.-X. Li, Z.-J. Lin, M.-L. Tong *Cryst. Growth Des.* **2007**, 7, 2352. (c) Z.-M. Hao, J. Wang, X.-M. Zhang. *CrystEngComm* **2010**, 12, 1103.

25. (a) F. B. Stocker, M. A. Troester, D. Britton. *Inorg. Chem.* **1996**, 35, 3145. (b) F. B. Stocker, M. A. Troester. *Inorg. Chem.* **1996**, 35, 3154. (c) F. Grifasi, M. R. Chierotti, C. Garino, R. Gobetto, E. Priola, E. Diana, F. Turci. *Cryst. Growth Des.* **2015**, 15, 2929.
26. (a) O. N. Kataeva, D. B. Krivolapov, A. T. Gubaidullin, I. A. Litvinov, L. I. Kursheva, S. A. Katsyuba. *J. Molec. Struct.* **2000**, 554, 127. (b) P. W. R. Corfield. *Acta Crystallogr., Sect. E* **2014**, 70, 281.
27. E. Solari, S. De Angelis, M. Latronico, C. Floriani, A. Chiesi-Villa, and C. Rizzoli, *J. Cluster Sci.* **1996**, 7, 553.
28. Parthenopoulos, D. A.; Rentzepis, P. M. *Science* **1989**, 245, 843.
29. A. S. Dvornikov, J. Malkin, P. M. Rentzepis. *J. Phys. Chem.* **1994**, 98, 6746.
30. A. S. Dvornikov, P. M. Rentzepis. *Res. Chem. Intermed.* **1996**, 22, 115.
31. S. Rath, M. Heilig, H. Port, J. Wrachtrup. *Nano Lett.* **2007**, 7, 3845-3848.
32. Y. C. Liang, A. S. Dvornikov, P. M. Rentzepis. *J. Mater. Chem.* **2000**, 10, 2477.
33. A. S. Dvornikov, E. P. Walker, P. M. Rentzepis. *J. Phys. Chem. A*, **2009**, 113, 13633.
34. M. A. Omary, J. C. F. Colis, C. L. Larochelle, H. H. Patterson. *Inorg. Chem.* **2007**, 46, 3798.
35. D. S. Tyson, C. A. Bignozzi, and F. N. Castellano. *J. Am. Chem. Soc.* **2002**, 124, 4562.
36. P. M. Graham, R. D. Pike. *Inorg. Chem.* **2000**, 39, 5121.
37. (a) Q. Wang, G. Guo, T. C. W. Mak. *Chem. Commun.* **1999**, 1849. (b) Z. Hao, X. Zhang. *Cryst. Growth Des.* **2007**, 7, 64. (c) R. J. Trovitch, R. S. Rarig, J. A. Zubieta, R. L. LaDuca, *Acta Crystallogr., Sect. E* **2007**, 63, m339. (d) C. Näther, M. Wriedt. *Dalton Trans.* **2009**, 46, 10125. (e) R. Peng, D. Li, T. Wu, X. Zhou, S. W. Ng. *Inorg. Chem.* **2006**, 45, 4035. (f) S. Liang, M. Li, M. Shao, X. He. *J. Mol. Struct.* **2008**, 875,

17. (g) W. R. Knapp, J. G. Thomas, D. P. Martin, M. A. Braverman, R. J. Trovitch, R. L. LaDuca. *Z. Anorg. Allg. Chem.*, **2007**, 875, 575.
38. G. A. Bowmaker, J. V. Hanna. *Z. Naturforsch. B* **2009**, 64, 1478.
39. SAINT PLUS: Bruker Analytical X-ray Systems: Madison, WI, 2001.
40. SADABS: Bruker Analytical X-ray Systems: Madison, WI, 2001.
41. G. M. Sheldrick, *Acta Crystallogr., Sect. A* **2008**, 64, 112.
42. C. B. Hubschle, G. M. Sheldrick, B. Dittick. *J. Appl. Cryst.* **2011**, 44, 1281.